CYCLOOCTENE NITRILE DERIVATIVES AND THEIR SPECTRAL INVESTIGATION WITH ADVANCED NMR TECHNIQUES

Maryam SADRI

Master Thesis
Department of Chemistry
Behalf of Organic Chemistry
Prof. Dr. Cavit KAZAZ
2016

UNIVERSITY OF ATATURK
GRADUATE SCHOOL OF NATURAL AND APPLIED SCIENCES

MASTER THESIS

CYCLOOCTENE NITRILE DERIVATIVES AND THEIR SPECTRAL INVESTIGATION WITH ADVANCED NMR TECHNIQUES

Maryam SADRI

DEPARTEMENT OF CHEMISTRY
Organic Chemistry

ERZURUM
2016

TURKISH REPUBLIC
ATATURK UNIVERSITY
GRADUTE SCHOOL of NATURAL and APPLIED SCIENCES

THESIS APPROVAL FORM

CYCLOOCTENE NITRILE DERIVATIVES AND THEIR SPECTRAL INVESTIGATION WITH ADVANCED NMR TECHNIQUES

This study, prepared by Maryam SADRI, under supervision of Prof. Dr. Cavit KAZAZ, has been approved on the date of 14.... / 01.... / 2016. as Master Thesis, in the Department of Chemistry – Institute of Department of Organic Chemistry, by the below-named thesis committee with **majority/unanimously** (..../....).

President : Prof. Dr. Cavit KAZAZ — Signature :

Member : Prof. Dr. Ramazan ALTUNTAŞ — Signature :

Member : Yrd. Doç. Dr. Serdar BURMAOĞLU — Signature:

The above-mentioned result;

Has been approved in accordance with Institute Administrative Committee on the date of 18. /02. / 2016 and resolution number 8... /...62....

Prof. Dr. Ertan YILDIRIM

Institute Director

ÖZET

Yüksek Lisans Tezi

SİKLOOKTEN NİTRİL TÜREVLERİ VE İLERİ NMR TEKNİKLERİ İLE BUNLARIN SPEKTRAL İNCELENMESİ

Maryam SADRI

Atatürk Üniversitesi
Fen Bilimleri Enstitüsü
Kimya Anabilim Dalı
Organik Kimya Bilim Dalı

Danışman: Prof. Dr. Cavit KAZAZ

Bu tezde, Altundaş ve grubu tarafından sentezlenen bazı yeni siklookten nitril türevlerinin ileri NMR teknikleri ile yapısal karakterizasyonları belirlenmeye çalışıldı. Başlangıçta, amacımız 48°C sıcaklıkta ve bazik ortamda (çözücü olarak diklormetan) 3-bromo-8-chloro-cyclooct-1-enecarbonitrile **1** ve s-α-fenil-etilamin'in tepkimesinden **2** 8-Chloro-3-(1-phenyl-ethylamino)-cyclooct-1-enecarbonitrile **3** ve **4** bileşiklerini sentezlemekti. Ancak spektral veriler (^{1}H, ^{13}C, DEPT-135, DEPT-90, COSY, HMQC and HMBC) tamamıyla farklı bir molekülün yapısını gösterdi. Bu bileşiğin **DEHP** olduğu ve reaksiyon ortamına septadan ekstrakte olduğu anlaşıldı.

4-bromo-9-oxa-biyoclo [6.1.0] non-2-ene-2-carbontitrilin **10** sodyum azid ile olan reaksiyonundan elde edilen ürünlerin [**11** (**Z**) ve **Y**] yapıları ileri NMR teknikleri ile aydınlatılmaya çalışıldı.

2016, 75 sayfa

Anahtar Kelimeler: İleri NMR teknikleri, ^{1}H, ^{13}C, DEPT-135, DEPT-90, COSY, HMQC, HMBC, DEHP, siklooktan türevleri.

ABSTRACT

Master Thesis

CYCLOOCTENE NITRILE DERIVATIVES AND THEIR SPECTRAL INVESTIGATION WITH ADVANCED NMR TECHNIQUES

Maryam SADRI

Atatürk University
Graduate School of Natural and Applied Sciences
Department of Chemistry
Behalf of Organic Chamistry

Supervisor: Prof. Dr. Cavit KAZAZ

In this thesis, synthesized by Altundaş and his group, the structural characterizations of some new cyclooctane nitrile derivatives were tried to be determined by advanced NMR techniques. Initially, our aim, in basic conditions and at 48°C degree (dichloromethane solvent), from the reaction of the 3-bromo-8-chloro-cyclooct-1-enecarbonitril **1** and S-α-phenyl-ethylamine **2** was to synthesize the compounds of 8-Chloro-3-(1-phenyl-ethylamino)-cyclooct-1-enecarbonitril **3** and **4**. However, spectral data (^{1}H, ^{13}C, DEPT-135, DEPT-90, COSY, HMQC and HMBC) indicated the structure of a completely different molecule. Later, it was understood that this molecule was **DEHP** extracted from the septa to the reaction environment.

The structures of the products [**11** (**Z**) and **Y**] obtained from the reaction of the 4-bromo-9-oxabicyclo [6.1.0]non-2-year-2-carbontitril **10** and the sodium azide were tried to be determined by advanced NMR techniques.

2016, 75 pages

Keywords: Advanced NMR techniques, ^{1}H, ^{13}C, DEPT-135, DEPT-90, COSY, HMQC, HMBC, DEHP, cyclooctane derivatives.

ACKNOWLEDGEMENTS

I would like to thank my supervisors Prof. Dr. Cavit KAZAZ, who not only have taught me a tremendous amount about the world of research and academia, but have also given me invaluable insight, encouragement and guidance over these past two years. I've had the pleasure of working in a very warm and welcoming environment, and it's truly thanks to the attitude and continuous support of my supervisors. I would also like the mention the support of Prof. Dr. Ramazan ALTUNDAŞ, Dr. Barış ANIL and Prof. Dr. Hamdullah KILIÇ who were not my supervisor but still managed to find the time to offer advice whenever I was stuck with my research.

It has been my great pleasure to be part of the Prof. Ramazan ALTUNDAŞ laboratory groups, the members of which have always been friendly and supportive. My thanks go out to İbrahim, Nejat, Büşra, Emine, Derya for all their help. I would also like to thank the support staff in the Chemistry Department at Atatürk University. And I would like to thank you the Science Institute for their time and their generosity and kind

For mass analyses, we are grateful to Uz. Adem ERTÜRK from Atatürk University, East Anatolian High Technology Research and Application Center (DAYTAM)

Finally, my many thanks to my parents, my sister, and my be loving husband and all my friends for their unfailing support, and for keeping me in touch. This would not have been possible without them.

Maryam SADRI
January, 2016

TABLE OF CONTENTS

ABBREVIATIONS and SYMBOLS

B_0 : static magnetic field

B_1 : applied magnetic field

B_{eff} : effective magnetic field

DEHP : bis(2-ethylhexyl) phthalate

E : energy

FID : free induction decay

HETCOR : heteronuclear correlation

COSY : Correlation Spectroscopy

HMBC : Heteronuclear Multiple-Bond Correlation Spectroscopy

HMQC : Heteronuclear Multiple Quantum Coherence

I : spin angular momentum

NMR : nuclear magnetic resonance

m : magnetic quantum number

T : temperature

T_1 : spin-lattice relaxation

T_2 : spin-spin relaxation

$T_{1\rho}$: spin-lattice relaxation in the rotating frame

T_d : dwell time

β_m : magic angle

γ : gyromagnetic ratio

δ : chemical shift

θ : flip angle

μ : magnetic moment

ν : precessional frequency

θ : shielding constant

ω : Larmor frequency

h : Planck's constant

LIST OF FIGURES

LIST OF SCHEME

LIST OF TABLES

1. INTRODUCTION

Nuclear magnetic resonance (NMR) spectroscopy is used in many different chemical contexts, from structure analysis of molecules, to structure determinations of small organic molecules, and analysis of mechanism in reaction systems. Since the first observation of NMR signals from paraffin (Purcell *et al.* 1946) and water (Binsch 1969), NMR spectroscopy has expanded to one of the major techniques in chemistry.

In the early 20th century, molecular structures were still two-dimensional, but a number of new techniques for structural analysis were being developed, mainly by physicists. X-ray crystallography made it possible to determine the three-dimensional structure of small organic compounds, as well as of macromolecules like proteins and nucleic acids.

An intrinsic property of X-ray crystallography is that it requires crystals of the sample. If the molecule does not crystallize, which is the case for most complex carbohydrates and membrane proteins, NMR spectroscopy is a good alternative. NMR spectroscopy can be used to analyze the structure of a molecule in solution and since most molecules occur and interact in aqueous solution that is an advantage. NMR spectroscopy has become one of the most common techniques for the determination of molecules structures and it is crucial in the analysis of complex carbohydrates.

Nuclear magnetic resonance (NMR) spectroscopy is an effective method for the determination of chemical structure and dynamics. It is a non-invasive technique that is able to provide analytical information without destroying the sample. The frequencies of the peaks in the NMR spectrum allow the identification of functional groups, while the intensity of the peak is related to the number of atoms with resonance at that frequency.

1.1. Theory of Nuclear Magnetic Resonance

Nuclear magnetic resonance (NMR) is a phenomenon in which nuclei with spin angular momentum orient and absorb and emit electromagnetic radiation when placed in a magnetic field (Friebolin 2008). NMR spectroscopy utilizes this phenomenon to noninvasively investigate the structures and dynamics of atoms and molecules. The number of protons and neutrons in the nucleus determines the magnitude of the spin angular momentum of a nucleus. To be observable by NMR, a nucleus must have a spin angular momentum (I), or spin, that results from an odd number of protons, neutrons, or both. If the sum of the protons and neutrons in the nucleus is odd, then the nucleus will have an " integer spin (I=1/2, 3/2, 5/2, etc.). If the number of protons and neutrons are both odd, then the nucleus will have an integer spin (I=1, 2, 3, etc.). Nuclei with a spin value of "have a spherical distribution of charge and nuclei with spin values greater than "have a non-spherical distribution of charge that results in a quadrupolar moment. Nuclei with an even number of protons and neutrons do not have a spin value (I=0) and are not observable by NMR (e.g. ^{12}C). Commonly observed nuclei such as ^{1}H, ^{13}C, ^{15}N, ^{19}F, and ^{31}P have a spin value of ". Nuclei with spin values greater than ½ spin such as ^{7}Li, ^{23}Na, ^{27}Al, and ^{33}S pose more challenges to data collection due to the line-broadening quadrupolar interactions. The spin angular momentum has discrete values determined by the magnetic quantum number, m, which has values of (I, I-1… -I). This means there are 2I+1 possible state form. For nuclei with I=½, the values of m are ±½. (Noda 1986).

NMR active nuclei have an angular momentum, P, as a result of their motion in a loop. The angular momentum is related to the spin angular momentum by a constant, &, shown in equation 1 this constant is equal to h/2π, where h is Plank's constant.

$$P = \hbar\sqrt{I(I+1)} \tag{1.1}$$

Because nuclei are charged particles, they also have a magnetic moment; μ.This magnetic moment is a vector quantity, which has a discrete set of allowed values. The

magnetic moment is determined by the relationship to the angular momentum vector by an isotope-specific constant called the gyromagnetic ratio γ, in this equation 2:

$$\mu = \gamma P \tag{1.2}$$

The sign (+/-) of γ determines if μ is parallel (+) or anti-parallel (-) to P. The NMR detection receptivity of a nuclide is directly dependent on γ, where nuclei with large magnitudes of γ are relatively easy to detect, and nuclei with small magnitudes of γ are more difficult to detect.

In a static magnetic field, B_0, the magnetic moment favors parallel alignment with the field, as it is a lower energy orientation than anti-parallel alignment. This results in a net magnetic direction parallel to B_0. When the values of the quantum number are considered, the orientation of the spins is tilted slightly from absolute parallel orientation to the field as illustrated in Figure 1.1.

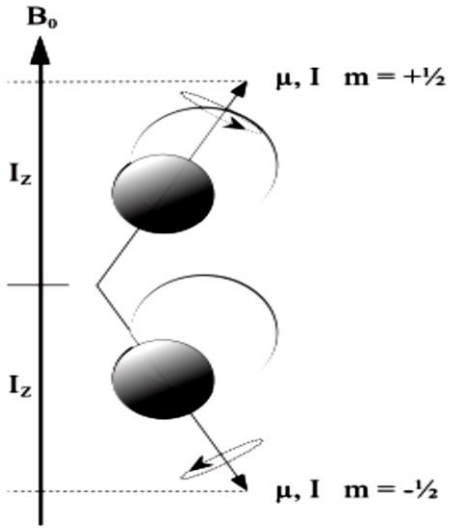

Figure 1.1. Orientations of the magnetic moment of a spin ½ nucleuses in an applied magnetic field (Noda 1986)

The slight angular offset from B_0 causes the magnetic moment and spin angular momentum vectors to precess around B_0 at a fixed frequency known as the Larmor frequency, ω, which is the product of γ and B_0, equation 3:

$$\omega = \gamma b_0 \tag{1.3}$$

Spins oriented both parallel and anti-parallel to B_0 precess around B_0 at the same Larmor frequency in a fixed magnetic field, as illustrated in Figure 1.2.

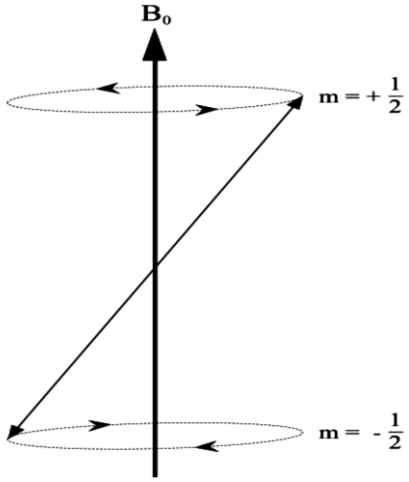

Figure 1.2. Larmor precession of nuclei in a fix magnetic field (Noda 1986)

The energy of a magnetic dipole in B_0 is defined by equation 4.

$$E = -\mu B_0 \tag{1.4}$$

In this equation, μ_z is the magnetic moment along the field direction, B_0 or z (equation 5).

$$\mu_z = m\gamma\hbar \tag{1.5}$$

Substituting equation 5 into equation 4, the energy level can be described by equation 6.

$$E = -m\gamma\hbar B_0 \tag{1.6}$$

Therefore a spin ½ system has spin states with energy equal to $\frac{\gamma\hbar B_\circ}{2}$ for m = - ½, higher energy, and - $\frac{\gamma\hbar B0}{2}$ for m = ½, lower energy (Bakhmutov. 2004). The difference in energy between these two states is $\gamma\hbar B_0$. In the absence of B_0, the states of I have the same energy, but in the presence of B_0 the energy levels split as seen in Figure 1.3.

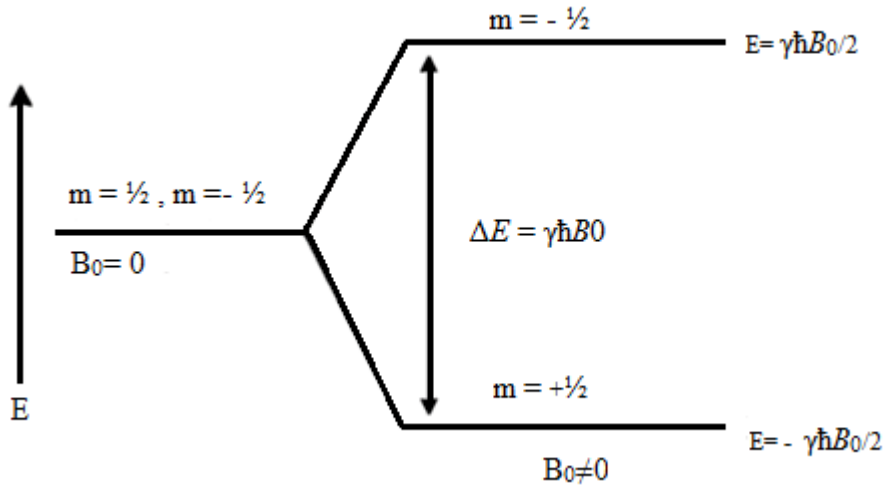

Figure 1.3. Energy level diagram for nuclei with I = ½ (Bakhmutov 2004).

The difference in energy between the two spin states, equation 7, is the magnitude of the magnetic moment and is related to the Larmor frequency substitution of equation 3.

$$\Delta E = \gamma\hbar B_0 = \hbar\omega \tag{1.7}$$

Transitions between spin states occur from the nucleus interacting with a magnetic field that oscillates at the precessional frequency (Bloch *et al*. 1946). The allowed transitions in NMR are restricted to those between adjacent energy levels, +m = ±1. These

transitions occur when electromagnetic radiation is introduced into the system. Electromagnetic radiation has characteristics of both a particle and a wave. The wave component consists of two orthogonal waves that oscillate in phase that corresponds to the electric and magnetic field vectors. The particle component, or photon, has an energy that is directly proportional to its frequency. The frequency of the oscillating magnetic field of the photon must match the Larmor frequency of the nuclei so that the nuclei can absorb energy from the electromagnetic wave. When this condition is met, the system is in resonance. When the electromagnetic field is in resonance and applied perpendicular to B_0, the nucleus absorbs energy from the wave and undergoes a transition of $+m = \pm 1$, as illustrated in Figure 1.4.

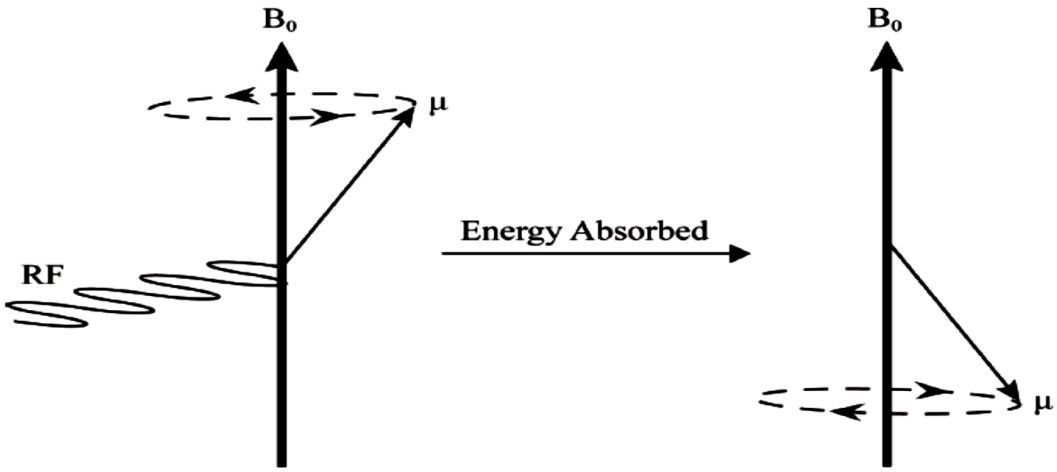

Figure 1.4. Transition of the magnetic moment upon absorption of a photon (Bloch *et al.* 1946).

When aligned parallel to B_0, the magnetic moment is in the "spin up" position. After absorption of a photon, the magnetic moment transitions to an anti-parallel, or "spin down" position. In the absence of a magnetic field, all orientations of nuclear spins are possible. The individual magnetic moments therefore have random orientations with no overall net magnetization (Figure 1.5 **A**). When a magnetic field is applied, spins favor alignment with the field. The sum of the magnetic moments is therefore in the direction of B_0. This sum creates a net magnetization parallel to B_0 (Figure 1.5 **B**) due to the slight excess of spins in the lower energy state.

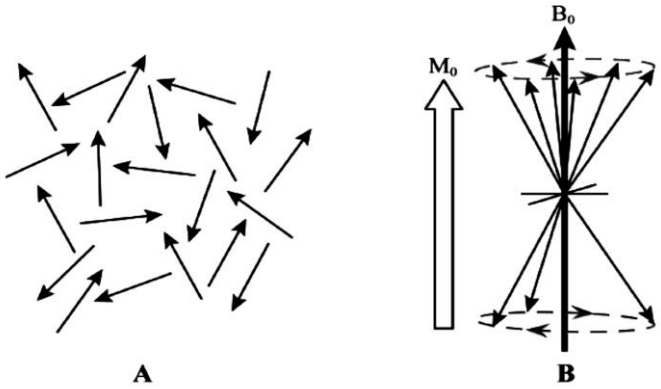

Figure 1.5. Magnetic moment vectors in the (**A**) absence and (**B**) presence of B_0, showing the net magnetization, M_0. (Paudler 1971)

In B_0 without interactions between spins, the initial population of the energy levels is described by the Boltzmann distribution (Paudler 1971). The Boltzmann population is described by equation 8 that relates the energy gap between the spin states, ΔE, to the relative population in each state.

$$\frac{N_+}{N_-} = e^{\frac{-\Delta E}{KT}} = e^{\frac{-\gamma \hbar B_\circ}{KT}} \tag{1.8}$$

In this equation, N_- is the number of spins in the higher energy level, N_+ is the number of spins in the lower energy level, T is temperature in Kelvin and k is the Boltzmann constant. The substitution of equation 7 into equation 8 shows the population difference to also be dependent of the gyromagnetic ratio and the field strength. Hypothetically, when electromagnetic radiation at resonance is applied all nuclear spins flip, as illustrated in Figure 1.6 (Grant 1996).

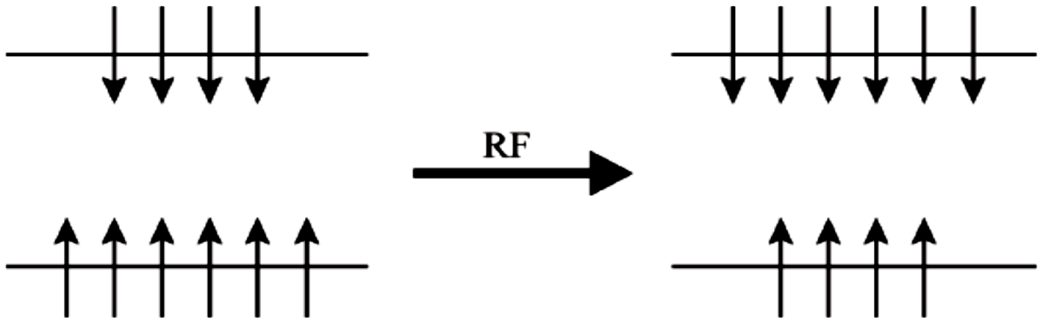

Figure 1.6. Theoretical flipping of a spin system upon application of electromagnetic radiation on resonance (Grant 1996)

In practice, not all spins in a spin state flip. The number of spins that flip is proportional to the population in that spin state. The population of the ground state decreases as the population of the higher state increases during absorption of electromagnetic radiation. This population shift continues until there is no longer an excess of spins in the ground state. Absorption of electromagnetic radiation ceases when the populations of the higher and lower energy levels are equal. This state is known as the saturated state, which is a non-equilibrium state. Upon reaching saturation, the spins return to the equilibrium state defined by the Boltzmann distribution through relaxation. The two methods of relaxation are spin-lattice and spin-spin relaxation, which are discussed further in section 1.2. NMR active nuclei precess at a unique frequency, ν, regulated by γ, equation 9 (Duer 2004).

$$\nu = \frac{\omega}{2\pi} = \frac{\gamma B_{\circ}}{2\pi} \tag{1.9}$$

To observe nuclei with an NMR spectrometer, the operating frequency, B_1, or the magnetic field strength, B_0, must be varied. Modern NMR methods use pulse-mode techniques where B_0 is held constant and the electromagnetic radiation is supplied through radio frequency (R_f) and R_f radiation by way of computer-controlled pulses of RF current (Bakhmutov 2004). This pulse operates at a single frequency that is centered at the operating frequency and is characterized by a power level and pulse width. The pulse covers a limited range of frequencies for a given power and width. The closer a

nucleus's precessional frequency is to the center of this applied pulse, the more energy the nucleus receives and the greater the spins deviate from alignment with B_0. This deviation is characterized by the angle between the spins and B_0, or the flip angle Θ. The short (μs) pulse of R_f radiation produces a field, B_1, perpendicular to B_0 that changes the direction of the net magnetization of the spins. This causes the spins to precess about B_0 and B_1. The illustration of the nuclear spins in B_0 can be simplified using the rotating axis frame. Figure 1.7 compares the static laboratory frame and the rotating axis frame.

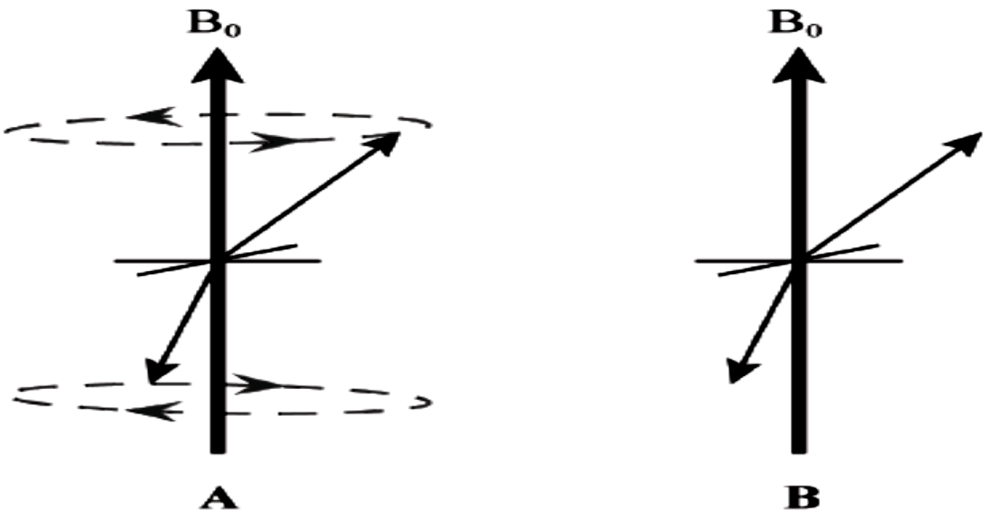

Figure 1.7. Nuclear spin vectors illustrated using the (A) laboratory and (B) rotation axis frame (Bakhmutov 2004)

In the laboratory axis frame, the axes are stationary and the net magnetization and nuclear spin vectors rotate around B_0 (z-axis) at the Larmor frequency. In the rotating axis frame, the xy plane rotates about the z-axis, B_0, at the Larmor frequency. This causes nuclear spin vectors to appear stationary. The spin system in B_0 favors alignment in the direction of the field. This means there is an excess of spin up nuclei over spin down nuclei. To simplify the illustration of the effect of B_1 on the spins, the net magnetization vector, M_0, is used, as shown in Figure 1.8.

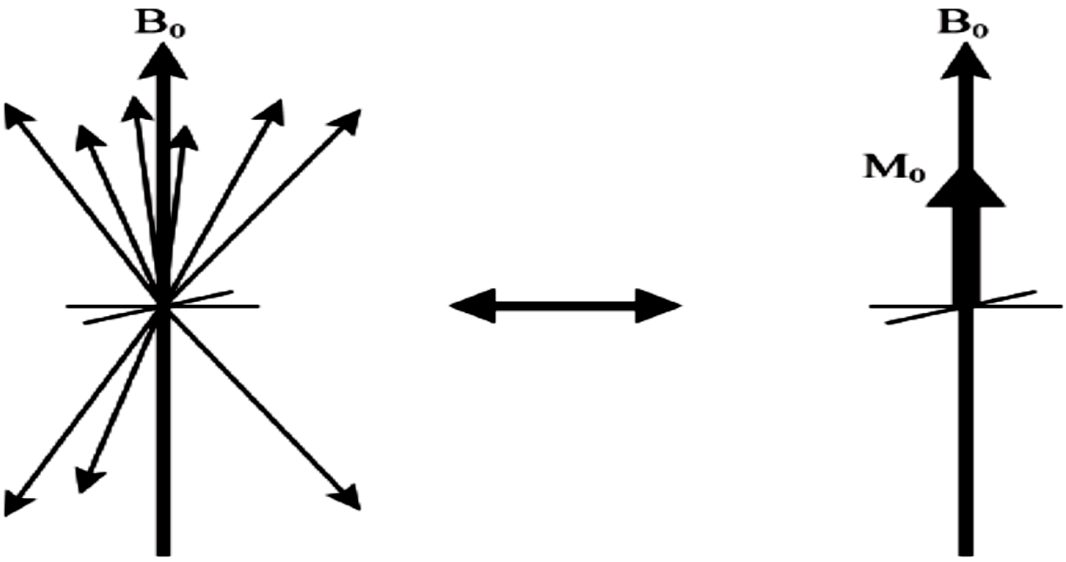

Figure 1.8. Net magnetization, M_0, along B_0 (Becker 1969)

The flip angle of M_0 depends on the gyromagnetic ratio, γ, the pulse field strength, B_1, and pulse width, or duration, t_p, described in equation 10 (Becker 1969).

$$\theta = \gamma B_1 tp \tag{1.10}$$

The magnetic moments of the nuclei begin aligned with B_0 along the z-axis. When an RF pulse is applied, the magnetic moments of the nuclei align and process about B_1 in such a way to flip M_0 into the xy plane where it processes with a frequency, ω_1, which is shown to be directly proportional to B_1 in equation 11.

$$\omega_1 = \gamma B_1 \tag{1.11}$$

The NMR spectrometer measures the magnetic moment about B_1 with a solenoidal (solid state) or saddle (solution state) coil detector located in the xy plane along the y-axis, as illustrated in Figure 1.9.

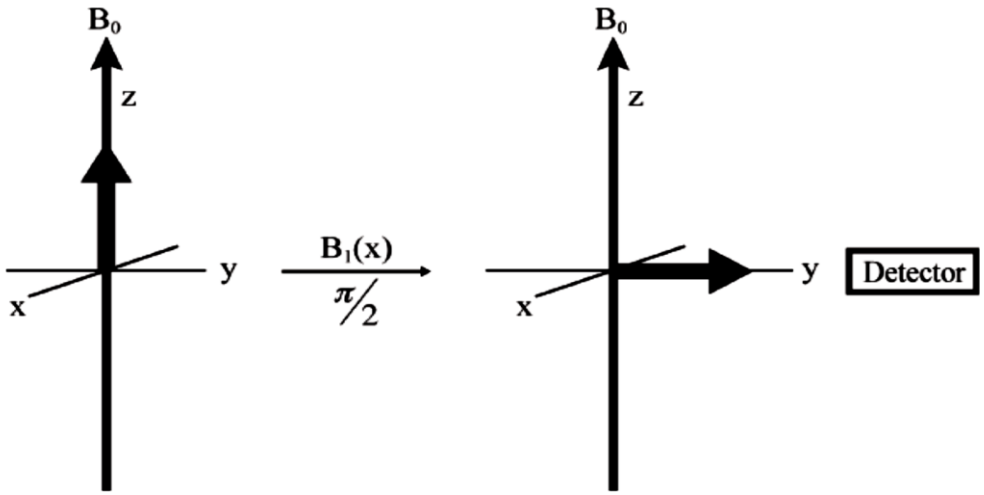

Figure 1.9. Observation of an NMR signal after application of B_1 (Becker 1969)

The precession of M_0 at ω_1 produces an oscillating current in the detector coil that creates an alternating current of the same frequency in the circuitry of the coil (Shaw 1984). The current is measured to generate a free induction decay (FID) over a period of time (Figure 1.10 **A**). The FID is a sum of all the signals with frequencies from each unique NMR active nucleus in the sample. A Fourier transform of the FID separates the frequencies into peaks on an axis with units of frequency where each peak is centered at its corresponding frequency in the FID (Figure 1.10 **B**).

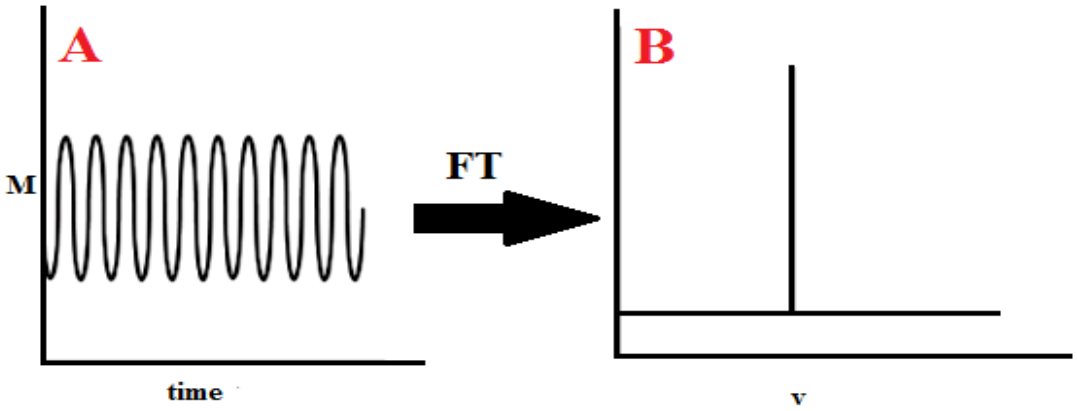

Figure 1.10. The (**A**) FID, and (**B**) the spectrum produced from the Fourier transform of an FID (Shaw 1984)

The induced signal is monitored as function of time through periodic measurement of the voltage in the coil. The time between measurements is determined by the dwell time, t_d. The limit of td is governed by the Nyquist Theorem, which states that in order for the instrument to determine the frequency of each magnetic moment it must acquire at least two points per cycle for the highest frequency component. Without relaxation of the spins, the magnetic moment along the y-axis would remain constant and the FID would extend infinitely in time. This would result in an infinitely narrow line in the Fourier transformed data as shown previously in Figure 1.10. In practice, the spins relax to equilibrium after the pulse so that the net magnetization realigns with B_0. This causes the magnetization along the y-axis to decrease exponentially with time (Becker 1969). The exponential decay of the FID changes the previous, infinitely narrow peak in the Fourier transformed data to appear as a Lorentzian shaped peak in the NMR spectrum (Figure 1.11).

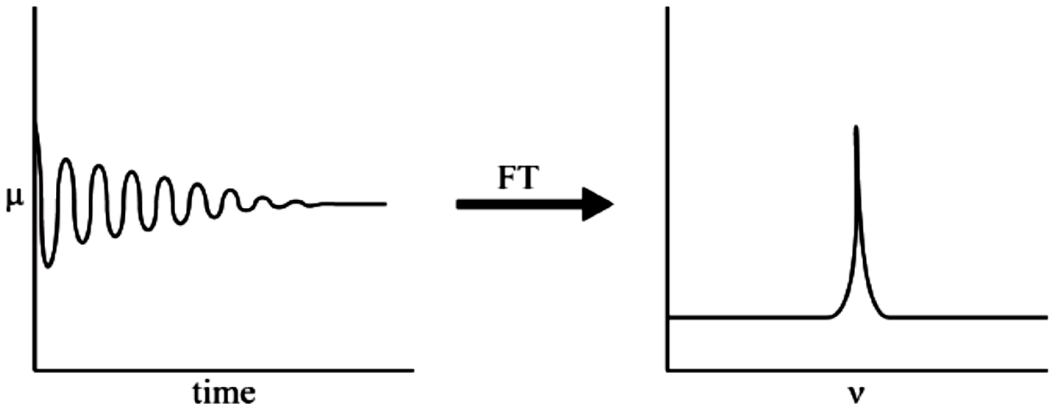

Figure 1.11. Fourier transform of an exponentially decaying FID due to relaxation (Becker 1969).

1.2. Relaxation

Relaxation in NMR refers to the processes through which a spins in the excited state return to the ground state until the system is at its equilibrium distribution. The two relaxation mechanisms are spin-lattice and spin-spin relaxation.

1.2.1. Spin-lattice relaxation

After absorption of R_f energy, the nuclear spins align perpendicular to B_1 within the xy-plane, which is perpendicular to B_0. Through relaxation processes, the net magnetization of these spins returns to alignment along B_0. The two relaxation mechanisms are spin-lattice (longitudinal) and spin-spin (transverse) relaxation. In spin lattice relaxation, fluctuations in the magnetic field at the nucleus allow the nuclear spins to transfer energy to the surrounding environment, or the lattice, and return to equilibrium value M_0 along B_0. When B_1 is turned off, the net magnetization returns to the Boltzmann distribution at a rate R_1 dependent on a time constant of T_1. The T_1 mechanisms used to transfer energy back to the lattice are dipole-dipole (DD), quadrupolar (Q), chemical shift anisotropy (CSA), scalar coupling (SC), and spin-rotation (SR) interactions. The combination of these interactions defines the T_1 relaxation time for a nucleus.

Dipole-dipole coupling refers to the through-space interactions between nuclear magnetic moments. As will be discussed in more detail later, the magnitude of this interaction is inversely dependent on distance between nuclei and is strongest for directly bonded nuclei. As the molecule moves, this interaction causes the local magnetic field detected at a nucleus to fluctuate, leading to relaxation. The stronger the dipolar coupling, the more effective the dipole-dipole relaxation will be. The rate of relaxation by dipole- dipole interactions is dependent on γ and the dipolar-coupling constant, as defined by equation 12, where *r* is the distance between two nuclei, and ħ is Plank's constant (Farra 1971).

$$R_{1\,(DD)} = \frac{1}{T^1(DD)} = \frac{2\hbar^2\gamma^4 I(I+1)}{5r^6} = \left[\frac{\tau}{1+\omega^2\tau^2} + \frac{4\tau}{1+4\omega^2\tau^2}\right] \quad (1.12)$$

In nuclei with spin values greater than I=½, the components of the quadrupolar coupling tensor become random functions of time, which changes the local magnetic field detected at the nuclei and leads to relaxation. The rate of this mechanism is dependent

on the magnitude of the quadrupole moment, Q, the electric field gradient, q_z, and the asymmetry of the electric field, η, as seen in equation 13:

$$R_{1\,(DD)} = \frac{1}{T^1(Q)} = \frac{3}{200}\frac{2I+3}{I^2(2I-1)}\left(1+\frac{\eta^2}{3}\right)\left(\frac{e^2Qqz}{\hbar}\right)^2\left[\frac{\tau}{1+\omega^2\tau^2}+\frac{4\tau}{1+4\omega^2\tau^2}\right] \quad (1.13)$$

Quadrupolar coupling is most effective for nuclei with large quadrupolar coupling constants. Nuclei with small quadrupolar coupling constants, such as ^2H and ^6Li, behave similarly to spin ½ nuclei. The chemical shift of the resonance of a nucleus is a function of the orientation of a nucleus in B_0. As the molecule tumbles in B_0, the resonance changes with the change in orientation of the nucleus. This causes the local magnetic field to change and leads to a relaxation at a rate defined in equation 14, where ($\sigma_{\shortparallel}$-$\sigma_{\perp}$) is the chemical shift anisotropy present (Farra 1971).

$$R_{1\,(DD)} = \frac{1}{T^1(CSA)} = \frac{1}{15}\gamma^2 B_\circ{}^2(\sigma_{\shortparallel}-\sigma_{\perp})^2\frac{2\tau}{1+\omega^2\tau^2} \quad (1.14)$$

When two nuclei α and β are coupled, the relaxation of the spins of α (S, with a short T_1 and S »½) can provide a relaxation pathway for the spins of β (I, where I = ½). Under these conditions, the rapid spin reorientation of the spins of α causes a rapid fluctuating magnetic field for the spins of β that allows it to exchange energy with the lattice. The rate of scalar coupling is defined in equation 15, where A is the spin-spin coupling constant and τ_s *S* are the relaxation time of nucleus S.

$$R_1{}^{I}{}_{(SC)} = \frac{1}{T^1(SC)} = \frac{2A^2}{3}S(S+1)\frac{\tau}{1+(\omega_i-\omega)^2\tau^2} \quad (1.15)$$

Spin rotation relaxation arises from the generation of local magnetic fields generated by the motion of the molecular magnetic moment. The change in molecular magnetic moment is a result of the circulation of electrons in the molecule. This type of relaxation is most dominant in small molecules and freely spinning functional groups such as methyl groups. The rate of spin rotation relaxation is given in equation 16, where C is

the spin-rotation tensor, k is the Boltzmann constant, and τ_J is the molecular reorientation correlation time.

$$R_{1\,(SR)} = \frac{1}{T_{1(SR)}} = \left(\frac{2\pi IKT}{\hbar^2}\right)\left[\frac{1}{3}(2C_{\perp}^2 + C_{\parallel}^2)\right]^2 \tau_J \quad (1.16)$$

The molecular reorientation correlation time is to τ_c by equation 17, where I is the moment of inertia of the molecule, k is the Boltzmann constant, and T is the absolute temperature.

$$\tau_J = \frac{I}{6KT\tau_c} \quad (1.17)$$

As temperature increases and the sample enters the gas phase, the molecular collisions become infrequent. In this state, the molecule remains at a given angular momentum state for a longer period of time. In addition, the molecule reorients more quickly with B_0 and shortens τ_c. This results in shorter T_1 spin-rotation relaxation times at higher temperatures and longer T_1 relaxation at lower temperatures, which contrasts the previous relaxation mechanisms (Farra 1971).

1.2.2. Spin-spin relaxation

In spin-spin relaxation, nuclei exchange energy with neighboring nuclei, which causes them to lose their phase coherence and disperse into a random arrangement around B_0 in the xy plane. The spin flip of a nucleus is simultaneous with the corresponding spin flip of a second nucleus, which maintains the energy of the system. Spin-spin, or T_2, relaxation is a result of molecular motion that causes fluctuations in the local magnetic field (Carlson 2010). Processes that contribute to T_1 relaxation also influence T_2 relaxation. Nuclei can precess around B_0 at frequencies greater or less than the Larmor frequency, which causes them to diphase, or fan out, in the xy plane over a time of T_2. T_2 relaxation is shorter than or equal to T_1 and governs the decay of the FID along with contributions from B_0 in-homogeneity. The line width of the peaks in an NMR spectrum

is related to T_2 and the magnet field in-homogeneity in equation 18 and illustrated in Figure 1.12.

$$\Delta\nu_{1/2} = \frac{1}{\pi T_2} + \gamma \frac{\Delta B_0}{2\pi} \tag{1.18}$$

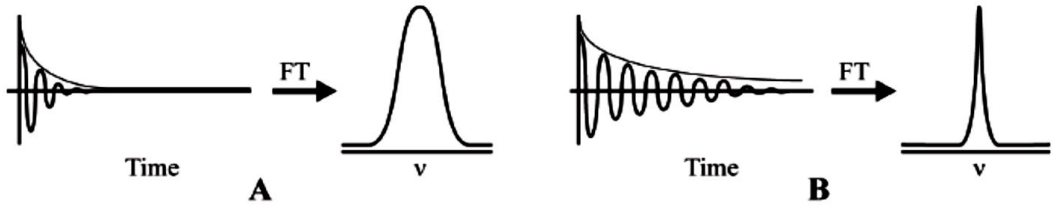

Figure 1.12. Resulting line widths from a system with (**A**) a short T_2 relaxation time producing a broad line width, and (**B**) a long T_2 relaxation time producing a narrow line width (Carlson 2010)

The T_2 relaxation time for a nucleus is defined by DD, Q, CSA, and SC interactions. The rates of relaxation for DD, Q, CSA, and SC interactions are defined by equations 19-22:

$$R_{2\,(DD)} = \frac{1}{T_{2(DD)}} = \frac{\hbar^2\gamma^4 I(I+1)}{5r^6}\left[3\tau_c + \frac{5\tau_c}{1+\omega^2\tau_c^2} + \frac{2\tau_c}{1+4\omega^2\tau_c^2}\right] \tag{1.19}$$

$$R_{2\,(Q)} = \frac{1}{T_{2(Q)}} = \frac{3}{400}\frac{2I+3}{I^2(2I-1)}\left(1+\frac{\eta^2}{3}\right)\left(\frac{e^2Qq_z}{\hbar}\right)^2\left[3\tau_c + \frac{5\tau_c}{1+\omega^2\tau_c{}^2} + \frac{2\tau_c}{1+4\omega^2\tau_c^2}\right] \tag{1.20}$$

$$R_{2\,(CSA)} = \frac{1}{T_{2(CSA)}} = \frac{1}{90}\gamma^2 B_0^2\left(\sigma_{\parallel} - \sigma_{\perp}\right)^2\left[\frac{6\tau_c}{1+\omega^2\tau_c{}^2} + 8\tau_c\right] \tag{1.21}$$

$$R^I_{2\,(CSA)} = \frac{1}{T^I_{2(SC)}} = \frac{A^2}{390}S(S+1)\left[\tau_S + \frac{\tau_S}{1+(\omega_I-\omega_S)^2\tau_S^2}\right] \tag{1.22}$$

Figure 1.13 illustrates T_2 relaxation using the rotating axis frame. When the RF pulse is turned on, it creates a rotating field, B_1, which appears stationary in the rotating frame, and the magnetization (M_0) appears to rotate in the plane perpendicular to B_1.

T_2relaxation causes decoherence in the net magnetization and the nuclear spins diphase about B_0 in the xy plane.

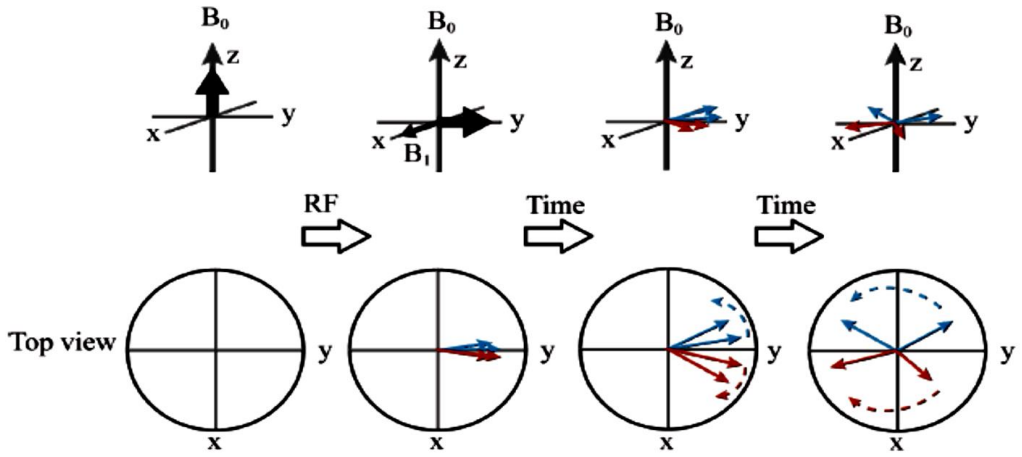

Figure 1.13. Dephasing of spins during T2 relaxation (Carlson 2010)

Relaxation also occurs in the applied B_1 field. This type of relaxation is known as T_1 in the rotating frame, or $T_{1\rho}$. $T_{1\rho}$ is equal to T_2 relaxation in non-viscous liquids. [19] In solids, $T_{1\rho}$ differs from T_2 due to the presence of static magnetic dipolar fields from neighboring nuclei. The dipolar field, B_d, usually dominates the effective field of a nucleus, B_{eff}. When B_1 is applied, $B_{eff} = B_d + B_1$. If $B_1 < B$, then T_1 and T_2 relaxation will dominate. If $B_1 \geq B_d$ then $T_{1\rho}$ will depend on B_1 with a rate defined by equation 23.

$$R_{1\rho}=\frac{1}{T_{1\rho}} = B_d^2\left[\frac{\tau_c}{1+4\omega_1^2\tau_c^2}\right] \tag{1.23}$$

Because the correlation time, τ_c, is multiplied by the precessional frequency in the rotating frame, ω_1, and not the Larmor frequency, the minimum of $T_{1\rho}$ is at a very different frequency than the minimum for T_1. This makes $T_{1\rho}$ measurements more suitable for studying lower frequency molecular motions (Harris 1986.). A comparison of the dependence of T_1, T_2, and $T_{1\rho}$ on τ_c is shown in Figure 1.14. Region A of Figure 1.14 represents the motional regime of non-viscous liquids where rapid tumbling averages anisotropic nuclear spin interactions and produces near identical relaxation

values, which are independent of field strength. For viscous liquids in region B, T_1 becomes larger than $T_{1\rho}$ and T_2 and begins to show dependence on the B_0 field. The non-rigid solids (region C) have T_1 values much larger than $T_{1\rho}$. $T_{1\rho}$ in this region is dependent on the strength of B_1 and is greater than T_2. The final region D represents the motional regime of rigid lattice solids, which have very short T_2 values and very long T_1 values. T_1 and $T_{1\rho}$ remain dependent on the B_0 and B_1 fields, respectively. T_2 relaxation shows a slight B_0 field dependency between regions C and D, but otherwise remains field independent and decreases in value as correlation time increases (Carlson 2010).

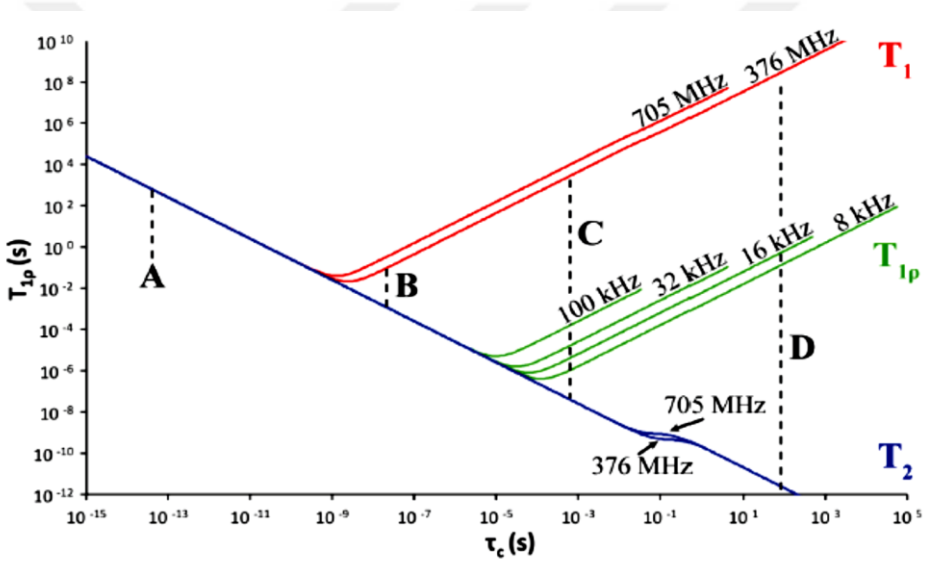

Figure 1.14. Dependence of relaxation times on molecular correlation time τ_c: (**A**) non-viscous liquid, $T_1 = T_{1\rho} = T_2$; (**B**) viscous liquid $T_1 > T_{1\rho} = T_2$; (**C**) non-rigid solid $T_1 >> T_{1\rho} \geq T_2$; (**D**) rigid lattice, $T_1 >> T_{1\rho} >> T_2$ (Carlson 2010).

1.3. Chemical Shift

The NMR frequency, or Larmor frequency, for a single isolated nucleus, is determined by γ and the strength of the magnetic field, as described in equation 3 (Klinowski. 2005). The frequency of the RF radiation absorbed by the nuclei is strongly affected by nearby electrons and nuclei and their distribution that comprise the chemical environment of the nuclei. The interaction with the chemical environment creates a unique precessional frequency for each nucleus in a different chemical environment. This leads to multiple peaks at different frequencies, or chemical shifts of the

resonances, in the NMR spectrum. Chemical shifts exist because the local field experienced by a nucleus differs from the external magnetic field, B_0. The difference is created by small magnetic fields formed by orbiting electrons around the nucleus. The local field, B_{loc}, opposes B_0 resulting in an effective field, B_{eff}, which is marginally different from B_0, as described by equation 24.

$$B_{eff}=B_0 - B_{loc} \tag{1.24}$$

Because the strength of the local field is directly proportional to the external field, a shielding constant,σ, is used to define the exact molecular environment of the nucleus. The shielding constant is dimensionless and field independent. Equation 25 shows the relationship between the resonance frequency, ν_1, and σ.

$$\nu_1=\frac{\gamma B_0(1-\sigma)}{2\pi} \tag{1.25}$$

The resonance frequency is directly proportional to B_0 and the shielding factor (1- σ). This means that nuclei, which are not chemically equivalent, are shielded to different

Amounts and produce different resonance signals in the NMR spectrum. To simplify spectral interpretation, regardless of NMR field strength, the chemical shift term, δ, is used. The chemical shift, δ, is a dimensionless, field-independent molecular property that defines the difference between the resonance frequency of the nucleus of interest, ν, and the reference nucleus, ν_{ref}, as defined in equation 26 (Klinowski 2005).

$$\delta=\frac{10^6(\nu-\nu_{ref})}{\nu_{ref}} \tag{1.26}$$

In the absence of other influences, the shielding of nuclei in organic structures will decrease with increasing electro-negativity of adjacent groups. The shielding in inorganic systems is influenced by the oxidation state. A nucleus with a higher value of

δ is referred to as fewer shields and a nucleus with a lower value of δ is referred to as more shield.

1.4. One-Dimensional NMR

NMR experiments are carried out by applying a strong radiofrequency pulse with a short duration (microseconds) close to the resonance frequency. The magnetization is pushed from the *z* axis towards the *y* axis (a 90° pulse) or, for a longer pulse, further to the -*z* direction (a 180° pulse). The induced magnetization along the *y* axis is detected as the free induction decay (FID), (Blümich 2005). This time domain function is converted into the frequency domain (the spectrum) by a Fourier transformation FT (Figure 1.15).

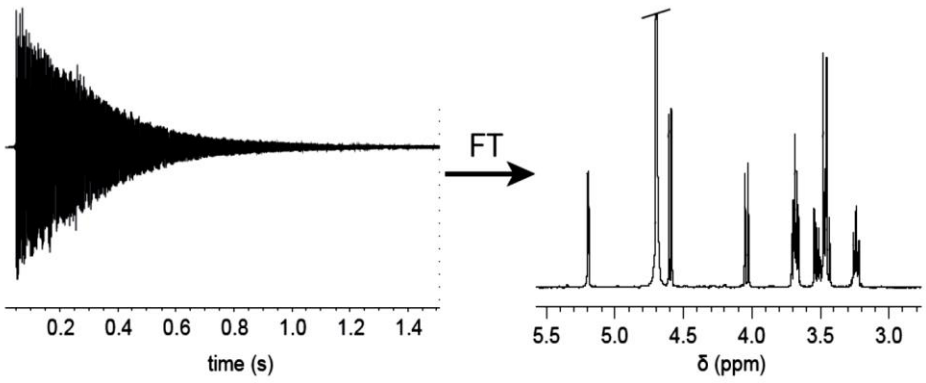

Figure 1.15. Signals in the time domain (FID) and in the frequency domain from a ^{1}H NMR experiment of glucuronic acid in deuterated water (D_2O).
*The truncated signal at 4.7 ppm originates from HDO (Blümich. 2005)

The information that can be extracted from a ^{1}H NMR spectrum is not restricted to the chemical shift, which is used to determine the chemical surrounding of a proton due to differences in electronic shielding, but also involves coupling constants, the line width, and the relative intensities of the signals (Figure 1.16).

Coupling constants have their origin in the influence of neighboring spins on the nucleus being observed. This scalar spin-spin coupling is transferred through the

electrons of chemical bonds and can yield additional structural information. Scalar coupling constants can be homonuclear or heteronuclear (Myers 1973).

The one-bond scalar coupling between ^{1}H and ^{13}C ($^{1}J_{CH}$) is only visible in a ^{1}H-NMR spectrum as small ^{13}C satellites, due to the low abundance of ^{13}C and ^{12}C being magnetically inactive (Spin=0). On the other hand, homonuclear ^{1}H-^{1}H coupling strongly affects the spectrum by splitting of the signals into multiplets. The area under a ^{1}H-NMR signal is proportional to the abundance of that proton in the sample (Abragam 1983). This is essential in structural analysis and makes quantitative NMR possible.

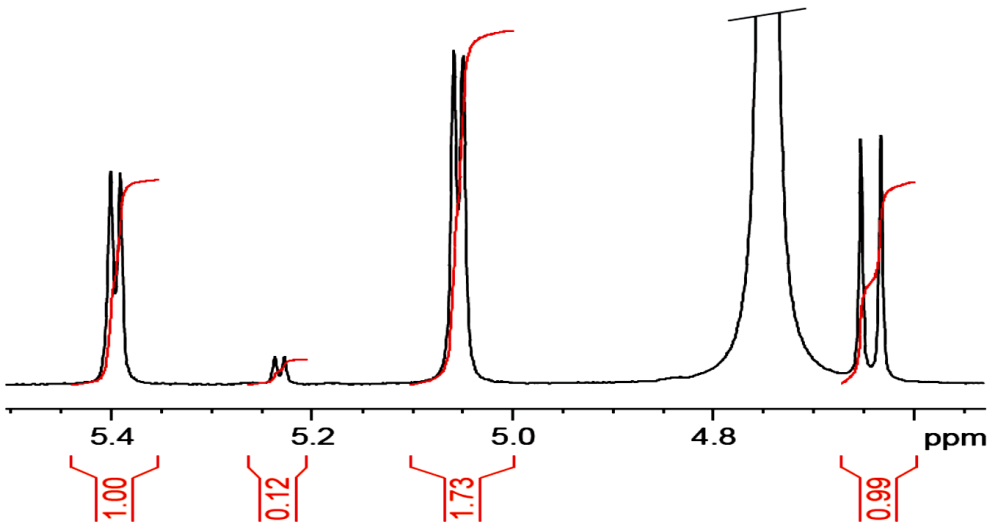

Figure 1.16. The anomeric region of a ^{1}H-NMR spectrum of a mixture of maltose and β-cyclodextrinin D_2O, shows signals with differences in chemical shifts, coupling constants, and intensities
*The truncated signal at 4.75 ppm originates from HDO (Abragam 1983).

The one-dimensional NMR spectrum shows amplitude as a function of frequency. To generate this spectrum, an ensemble of a particular NMR-active nuclide is excited. The excited nuclei generate a signal that is detected in the time domain and then converted mathematically to the frequency domain by using a Fourier transform.

Older instruments called continuous wave (CW) instruments do not simultaneously excite all the spins of a particular nuclide. Instead, the magnetic field is varied while R_f

of a fixed frequency is generated. As various spin populations come into resonance, the complex impedance of the NMR coil changes in proportion to the number of spins at a particular field and R_f frequency (Dixon 1972). Thus, we can speak of observing a resonance at a particular point in a spectrum we collect. This process of scanning the magnetic field is slow and inefficient compared to how today's instruments work, although there is a certain aesthetic appeal in the intuitively more obvious nature of the CW method.

All 1-D NMR time domain data sets must undergo one Fourier transformation to become an NMR spectrum. The Fourier transformation converts amplitude as a function of time to amplitude as a function of frequency. Therefore, the spectrum shows amplitude along a frequency axis that is normally the chemical shift axis.

The signal we detect to ultimately generate a 1D-NMR spectrum is generated using a pulse sequence. A pulse sequence is a series of timed delays and R_f pulses that culminates in the detection of the NMR signal. Sometimes more than one R_f channel is used to perturb the NMR-active spins in the sample. For example, the effect of the spin state of ^{1}H's on nearby ^{13}C's is typically suppressed using ^{1}H decoupling (proton decoupling) while we acquire the signal from the ^{13}C nuclei (Hennel 1993).

Figure 1.17 shows a simple 1D-NMR pulse sequence called the one pulse experiment. The pulse sequence consists of three parts: relaxation, preparation, and detection. A relaxation delay is often required because obtaining a spectrum with a reasonable signal-to-noise ratio often requires repeating the pulse sequence (scanning) many times to accumulate sufficient signal, and following preparation (putting magnetization into the xy plane), the NMR spins will often not return to equilibrium as quickly as we might like, so we must wait for this return to equilibrium before starting the next scan. Some relaxation will take place during detection, but often not enough to suit our particular needs.

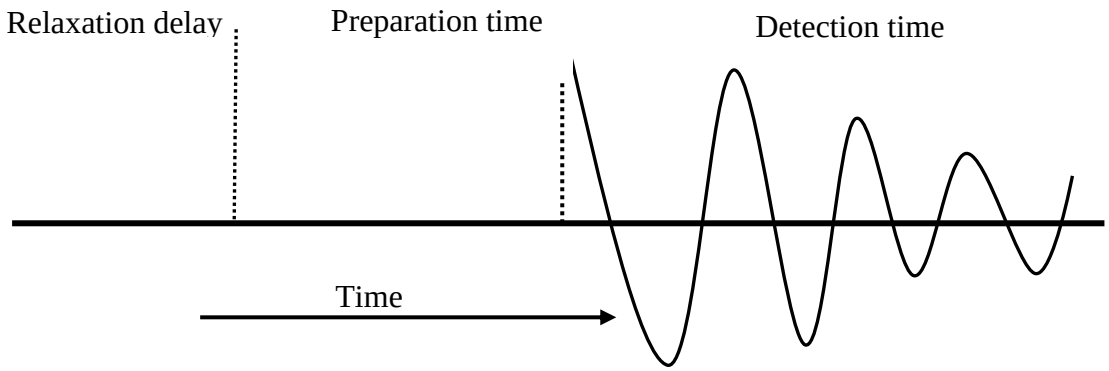

Figure 1.17. The three distinct time periods of a generic 1D-NMR pulse sequence (Hennel *et al.* 1993)

1.5. Two-Dimensional NMR

To correlate the resonances of two nuclei in a molecule, two dimensional (2D) NMR can be used. Two dimensions here refer to two frequency domains. Ever since the first 2D-NMR experiment reported by Ernst et al, extensive 2D-NMR applications have been developed and used to study the complex molecule such as synthetic polymers. All the 2D-NMR experiments have the same basic format which can be divided into four units: preparation, evolution, mixing and detection periods (Keeler 2004).

In a manner similar to the 1D experiment, the preparation period usually starts with a delay during which the spins are allowed to return to equilibrium; this is followed by a pulse or a cluster of pulses and delays that places the magnetization in the x-y plane, just before the evolution period.

The evolution period (t_1) is a variable time delay, increased in a stepwise manner from an initial value of zero to a final value ni x 1/sw (related with spectral window sw1 in the indirectly detected dimension), which provides the key to the generation of the second dimension.

The mixing period also contains a pulse or a cluster of pulses, during which the magnetization is transferred from one nucleus to another. The detection (t_2) period is needed to collect the FID data. It produces a spectrum similar to the one obtained from a 1D experiment of the detected nucleus. The general scheme for any 2D experiment is shown in Figure 1.18 (Keeler 2004).

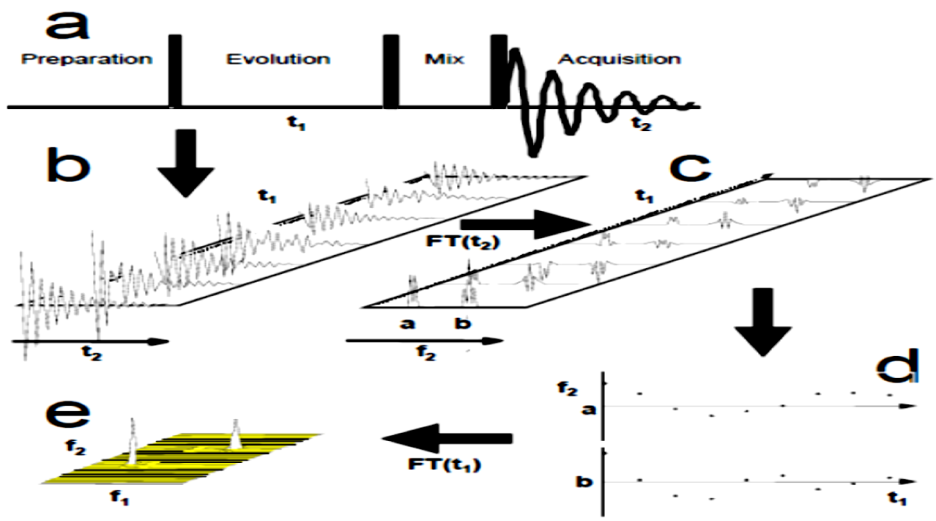

Figure 1.18. Schematic of 2D-NMR data collection and processing (Noda 1986).

Each t_1 value in the 2D sequence is repeated n_t times and n_p data points (FID) is stored. (n_p is related to the acquisition time at, and s_w is the direct detection dimension spectral window).

For each FID, the t_1 delay is incremented; the magnetization in the transverse plane is allowed to evolve for progressively longer times, leading to amplitude modulation of the FIDs collected during the detection period t_2 as shown in Figure 1.18 **b**.

Fourier transformation of t_2 FIDs produces a series of spectra containing resonances whose intensity varies as a function of time t_1. If the peak intensities at each position in f_2 are plotted as function of t_1; as shown in Figure 1.18 **c**, the intensity of resonances as a function of time represents another set of free induction decays that has been

generated artificially as in Figure 1.18 **d**. Fourier transform of these time domain data with respect to t_1 produces resonances plotted along the f_1 frequency dimension. The final Fourier transformed 2D-NMR spectrum is presented in Figure 1.18 **e**, showing a stacked plot of the signal intensity correlated to two frequencies in dimensions f_1 and f_2 (Noda 1986).

There are two basic types of 2D-NMR experiments, homonuclear correlation experiments which correlate shifts of two similar spins (e.g. ^{1}H with ^{1}H); and heteronuclear correlation experiments which correlate different spins. The most applicable homonuclear experiments are **CO**rrelation **S**pectroscop**Y** (COSY), **TO**tal **C**orrelation **S**pectroscop**Y** (TOCSY), **N**uclear **O**verhauser **E**ffect **S**pectroscopY (NOESY). The typical examples of **HET**eronuclear experiments are heteronuclear **COR**relation spectroscopy (HETCOR), **H**eteronuclear **M**ultiple-**Q**uantum **C**orrelation (HMQC), **H**eteronuclear **S**ingle-**Q**uantum **C**orrelation (HSQC), **H**eteronuclear **M**ultiple-**B**ond **C**orrelation (HMBC) (Noda 2008).

The simplest pulse sequence for 2D-NMR is COSY, presented in Figure 1.19, which normally correlates the same spectral windows in the f_1 and f_2 dimensions and are symmetrical about their diagonal. COSY produces a spectrum with peaks along the diagonal (autocorrelation peaks), which indicate a nucleus' resonance correlated with itself. Off-diagonal correlations (cross-peaks) are observed between the resonances of nuclei (most often ^{1}H-^{1}H) through J-couplings. It is of great utility in the study of hydrocarbon based polymers (Katayama 2010).

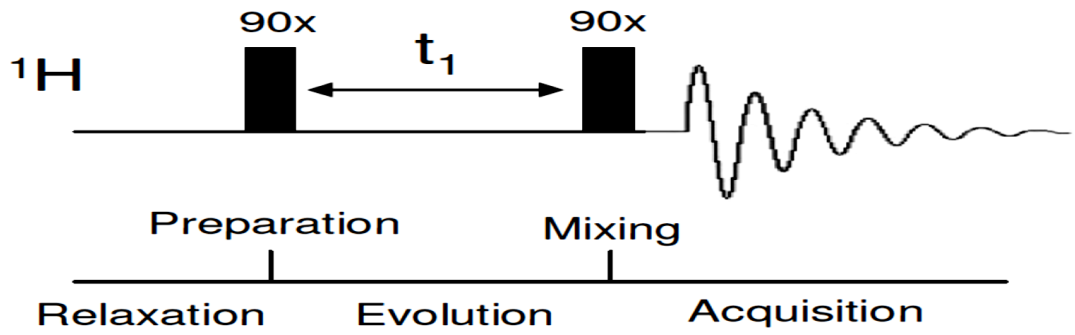

Figure 1.19. COSY pulse sequence (Katayama 2010)

Another example of a 2D-NMR experiment is the heteronuclear singlequantum correlation (HSQC) experiment. It normally produces a spectrum with correlations between shifts of nuclei with "high NMR receptivity" such as $^1H/^{19}F$ and nuclei with "low NMR receptivity" such as ^{13}C.

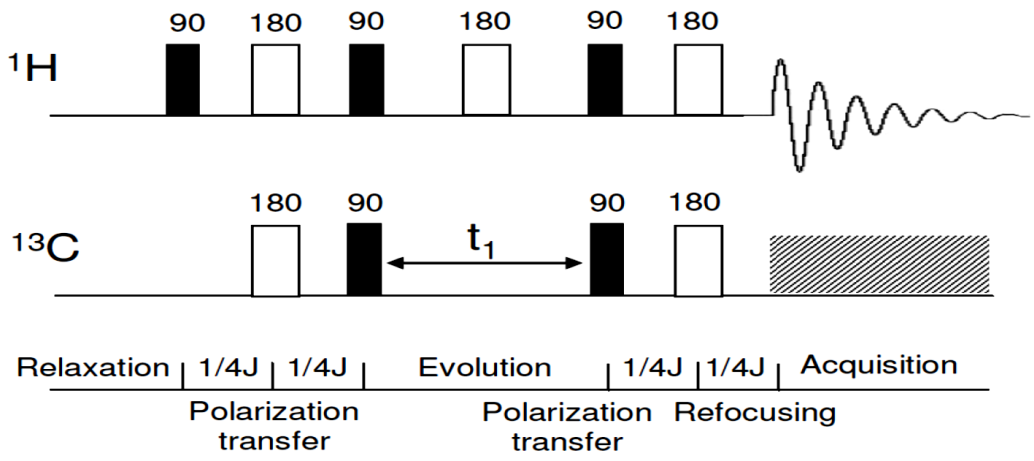

Figure 1.20. HSQC pulse sequence (Noda 2000).

In the basic HSQC pulse sequence displayed in Figure 1.20, the magnetization starts on ^1H atoms and is transferred to ^{13}C through INEPT. The spins precess at the ^{13}C frequency during the evolution time t_1. A ^1H 180° pulse in the middle of the t_1 period serves to remove ^1H-^{13}C couplings, so that only heteronuclear chemical shifts modulate the NMR signal in the f_1 frequency dimension. Finally, the heteronuclear magnetization

is transferred back to ^{1}H by a reverse INEPT step which ends with the two 90° pulses at the end of the t_1 period to produce anti-phase proton magnetization. The refocusing period realigns this antiphase magnetization for detection in the presence of ^{13}C-spin decoupling during t_2 acquisition time. The HSQC experiment can be obtained in a multiplet edited mode so that the cross-peaks from CH and CH_3 groups are positive and those from CH_2 groups are negative. This similar advantage has been seen in the DEPT experiment. In addition, HSQC has the greater sensitivity of ^{1}H detection and the dispersion associated with 2D-NMR (Noda 2000).

In general, HSQC provides cleaner spectra and better signal to noise ratio than another heteronuclear correlation experiment HMQC (Figure 1.21) which goes through multiple quantum coherence transfer. The basic HMQC sequence contains only four R_f pulses. The sequence starts with a proton 90º excitation pulse. Thus the proton spins are flipped to the transverse plane and precess for a delay controlled by the one-bond ^{13}C-^{1}H coupling. Antiphase proton magnetization develops during this time and is transferred to carbon by the subsequent carbon 90º pulse, which generates ^{13}C-^{1}H multiple quantum coherence. This coherence is a combination of both heteronuclear double- and zero-quantum coherences. Since the coherences contain terms for both transverse ^{13}C and ^{1}H magnetization, they will evolve under the influence of both ^{13}C and ^{1}H chemical shifts. To remove the effect of proton couplings and to reverse the effects of ^{1}H chemical shift evolution during evolution time, a 180° proton pulse is placed in the middle of t_1. By the end of the evolution time the proton-carbon couplings are refocused and thus have no influence in f_1. Evolution of the carbon shifts is unaffected by that proton 180º pulse. The final carbon pulse reconverts the multiple -quantum coherence back to observable single-quantum proton magnetization. A second ½ J period is inserted to refocus the proton antiphase components. During acquisition, decoupling on the ^{13}C channel is generally applied to remove ^{13}C-^{1}H coupling in f_2. Note that ^{1}H-^{1}H homonuclear J-couplings modulate the multiple quantum coherence in the t_1 period so that the signal in f_1 dimension contains both ^{13}C chemical shift information and is also split by J_{HH} couplings (Noda 2006).

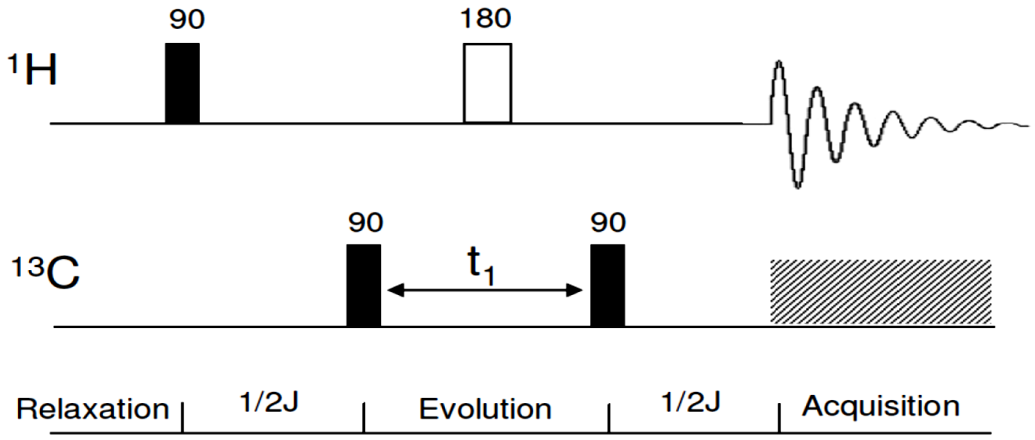

Figure 1.21. HMQC pulse sequence (Noda 2006).

HMBC (Figure 1.22) and HMBC experiments are applied when multiple-bond heteronuclear correlations are studied. The pulse sequence of HMBC is similar to the pulse sequence of HMQC. The first carbon 90° pulse creates multiple quantum coherence for the one-bond coupling while the second carbon 90° pulse creates multiple quantum coherence for the long-range couplings (set in delay tau). The one-bond correlation is suppressed and removed from the spectra by alternating the phase of the first carbon pulse. The carbon decoupler is turned off in this sequence. This is because there is no refocusing period for proton antiphase components after evolution time; therefore, the protons display both homonuclear and heteronuclear couplings. A refocusing period is absent because it is difficult to set a delay to optimally refocusing all of the $^{n}J_{CH}$ couplings which span an order of magnitude. Furthermore, the long delay needed to refocus small J_{CH} couplings would permit significant relaxation and as a consequence, less of signal intensity.

The latter factor is especially a problem when studying polymers which have short T_2's. This technique serves best when indirectly detecting quaternary carbons coupled to protons.

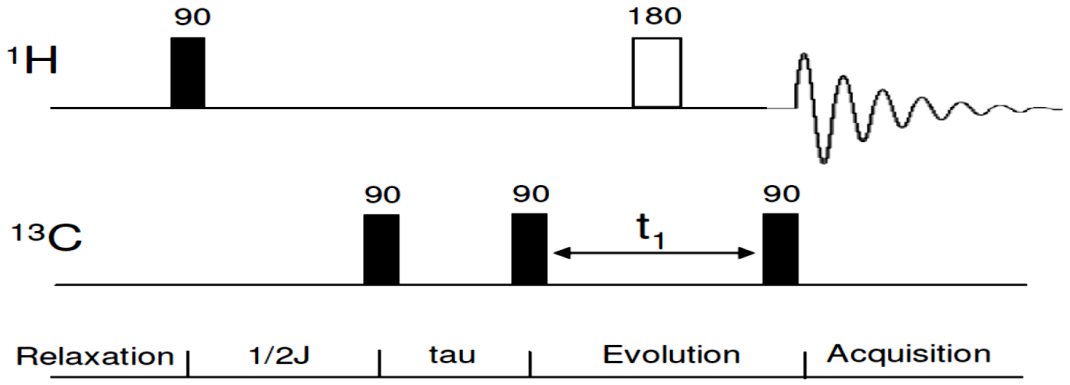

Figure 1.22. HMBC pulse sequence (Farrar *et al.* 1971)

HSQC and HMBC are useful techniques providing information about the skeleton of a molecule. However, there are disadvantages as well. For example, in HSQC, many pulses are used, especially the 180° pulses on the heteronuclear channel. The intensity can be lost from R_f in-homogeneity, pulse miscalibration or off-resonance excitation. Such losses need to be minimized by careful probe tuning and the use of composite or adiabatic 180º pulses. CRISIS and CRISIS-HSQC versions of the 2D-HSQC experiments use swept pulses as substitutes for simple 180° inversion pulses on the heteronuclear channel, and both ^{1}H and heteronuclear channels, respectively. These modifications could compensate for imperfect pulses and resonance offset effects, thus generally provide far better signal-to-noise than the simple versions of the pulse sequence (Farrar *et al.* 1971).

1.6. Variable Temperature Unit (VTU) Operation

Variable temperature NMR is an excellent way to investigate dynamic behavior of molecules. Both qualitative and quantitative information about inversion, ring-flip, and other barriers can be extracted from a series of spectra at different temperatures (Katayama 2010). VTU operation is available on many of spectrometers. In the **V**ariable **T**emperature **U**nit (VTU), it has usually set limits of 0 to 50 °C, these temperatures were selected to protect the probes from damage due to either a solvent freezing or cracking the NMR tube or a solvent boiling and spilling in the probe. High temperatures could

cause significant probe damage. Any compound can check in different temperatures and monitoring how it does behavior in high temperature.

In this study, advance NMR techniques combined with highly developed instruments were utilized to provide abundant information about primary our molecule structure. Starting with 1D-NMR which is confirm our molecule has symmetric structure and the counting of carbons and hydrogens, the 2D-NMR and experiments were carried to prove the connection between structure units. At least we determined our molecule has dynamic behavior or not.

2. LITERATURE REVIEW

Jing-Ying Shey (2002) "Liquid-phase combinatorial reaction monitoring by conventional ^{1}H- NMR spectroscopy", they studied on the online reaction mechanism with NMR technique, the application of ^{1}H-NMR spectroscopy for complete analysis of soluble polymer-supported reactions is described, to determine the extent of liquid-phase reactions without cleavage of the soluble matrix.

Sebastien Monfette *et al.* (2009) "Monitoring ring-closing metathesis: Limitations on the utility of 1H NMR analysis", they worked on the utility and limitations of ^{1}H-NMR methods for monitoring the progress of ring-closing metathesis (RCM) reactions are examined. They proved DOSY-NMR can aid in resolving ambiguities in signal assignment, but reliable quantitation requires ancillary methods.

Cardoza *et al.* (2004) "Applications of NMR spectroscopy in environmental science", it's very useful review of how to covers a number of applications of nuclear magnetic resonance (NMR) spectroscopy in the broad area of environmental science. In this review they collected the numerous of NMR techniques as new method to determine the environmental properties or contaminations.

Stockman (1998) "NMR spectroscopy as a tool for structure-based drug design", its review how to use NMR techniques one of two techniques, the other being X-ray crystallography, that can provide atomic-level descriptions of the intermolecular receptor-drug interactions responsible for molecular recognition.

Noda (2010) "Progress in two-dimensional (2D) correlation spectroscopy", this study is review about the 2D NMR, and Pertinent review articles and conference proceedings are discussed first, followed by the examination of noteworthy developments in the theory and applications of 2D correlation spectroscopy, in Application areas of 2D correlation spectroscopy are diverse, encompassing synthetic and natural polymers,

liquid crystals, proteins and peptides, biomaterials, pharmaceuticals, food and agricultural products, solutions, colloids, surfaces, and the like.

Noda (2015) "Recent developments in two-dimensional (2D) correlation spectroscopy", in this work recent noteworthy developments in the field of two-dimensional (2D) correlation spectroscopy are reviewed. 2D correlation spectroscopy has become a very popular tool due to its versatility and relative ease of use. The technique utilizes a spectroscopic or other analytical probe from a number of selections for a broad range of sample systems by employing different types of external perturbations to induce systematic variations in intensities of spectral.

Malet-Martino (2013) "NMR techniques in biomedical and pharmaceutical analysis", this article focuses on the description of some of the NMR techniques used in the field of biomedical and pharmaceutical research. The area of a NMR signal is directly proportional to the number of corresponding nuclei and thus, at variance with other techniques, the response factor is not dependent on the molecular structure.

Bernard *et al.* (2014) "Analytical methods for the determination of DEHP plasticizer alternatives present in medical devices: A review". This study worked on DEHP is plasticizer most commonly, in flexible plasticized PVC, phthalates are not chemically bound to PVC and they are released into the environment and thus may come into contact with patients. This review outlines recently analytical methods available to determine and quantify these plasticizers in several matrices, allowing the evaluation of potential risk and so risk management.

Ekelund (2010) "Evaporative loss kinetics of di (2-ethylhexyl) phthalate (DEHP) from pristine DEHP and plasticized PVC". This study is about the migration of di (2-ethylhexyl) phthalate (DEHP) from poly (vinyl chloride) (PVC) to a surrounding gas phase at temperatures below 120°C kinetically is controlled by evaporation. DEHP was accidently degraded as revealed by discoloration, the presence of low molar mass degradation products (liquid chromatography) containing additional carbonyl groups

(infrared spectroscopy) and an increase in the evaporation rate at temperatures between 100 and 130°C degree.

Özer (2012). "Determination of di (2-ethylhexyl) phthalate migration from toys into artificial sweat by gas chromatography mass spectrometry after activated carbon enrichment". These conditions were applied to study the migration of di (2- ethylhexyl) phthalate from different children's toys into artificial sweat. The detection limit of the method was 13.8 mg L^{-1}, while the relative standard deviation (%) value for the analysis of 100 μg L^{-1} of the analysis was below 3.7% (n=5).

Marcilla *et al.* (2003). "Study of the migration of PVC plasticizers". This study was about the capacity of migration of different commercial plasticizers from flexible PVC parts towards other media kept in contact with it; in this case, polystyrene (PS) has been used as example. The type of the plasticizer has also a significant effect and the citrates have higher migration capacity than phthalates.

Our aim, with advanced NMR techniques mentioned in detail from the theory, the structures of unknown compounds were to determine. However, to determine the structure of unknown compounds, NMR spectroscopy may not always be sufficient. In this case, we must also benefit from other spectroscopic methods. In the present thesis, synthesized by Altundaş and his groups, the structural characterization of some new cyclooctane nitrile derivatives were tried to determined with advanced NMR techniques, IR and mass.

3. MATERIAL and EXPERIMENTAL

3.1. Identify of the Cyclooctane Nitrile Derivatives

We aimed to study the structural elucidation of another cyclooctane nitrile derivatives, which are synthisized by Altundaş`s group as a part of Nejat Arçelik. For this puposes, advanced NMR techniques are used.

3.2. Instrument and Equipment

Spectrometer : Bruker 400 MHz
^{1}H frequency resonance : 400.0 Hz
^{13}C frequency resonance : 100.0 Hz
Magnetic field strength : 4
Resolution : 0.01
Probe : PFG
Cry magnet : Bruker
Computer : HP
Monitor : HP LP 2275
Printer : HP laser jet P2055dn
NMR tube : William Glass

Table 3.1. 1D and 2D NMR references

Solvent	Density	Temperature	Instrument	1D-NMR	2D-NMR
$CDCl_3$	20 mg/ml	20 °C	400 MHz	^{1}H, ^{13}C, DEPT	gHMBC, gHMQC, gCOSY

3.3. Samples Preparing

All the samples prepared in the WG-5mm (William Glass) tubes. Almost 10-15 mg of our compounds solved in 0.75 ml $CDCl_3$ (99.9%) Merck.

3.4. Experiments

The parameters and pulse sequences used in the 400 MHz Bruker and Varian instrument, for 1D-NMR and 2D-NMR as follow (400 MHz Bruker):

3.4.1. ^{1}H-NMR parameters (400 MHz Bruker)

GENERAL

DE (µs)……...….6.50	PLUPROG…… zg30
D1 (s)…….…..…1.00	TD……...….65536
TD0……...……1	NS…….…….16
Channel f1	DS…….…..…..2
NUC1……...…..1H	SWH (Hz)... ….....8223.68
P1 (µs)…….……....10.50	AQ (s)……..….3.9846387
PL1 (dB)…….……. -4.00	RG…….…..….40.3
PL1W (W) ….……..23.5978	DW (µs)…….…..…60.800

3.4.2. ^{13}C-NMR parameters (400 MHz Bruker)

GENERAL

RG…….…..…...32768	PLUPROG…… zgpg30
DW (µs)…….....…..20.800	TD……...……65536
DE (µs)……....….....6.50	NS…….…….3000
D1 (s)……...2.000	DS…….…….…..4
TD0……...…..……1	SWH (Hz)... ….....24038.46
Channel f1	AQ (s)…….1.3631988

PL2 (dB)…….…… -1.00
PL2W(W)…….....23.5978
NUC1…….……...…..13C
P1 (µs)…….……....10.00

3.4.3. DEPT parameters (400 MHz Bruker)

GENERAL
P2 (µs)…….……....20.00
PL1 (dB)…….……….. -1.50
PL1W (W) ….……...47.8998
SFO1 (MHz)….……100.6228
Channel f2
CPDPRG2…….……..waltz16
NUC2……..……1H
P3 (µs) ……....15
P4 (µs)……..30
PCPD2 (µs)……..……80
PL12 (dB)…….…….. -1.00
PL12W (W) ….……...0.3740
SFO2(MHz)….……400.13160
PLUPROG……..…… dept90
TD……...….….65536
NS…….……720
DS……..…….……..4
SWH (Hz)... ….....24038.46
AQ (s)…….1.3631988
RG……..…..….16384
DW (µs)…….……...…20.000
DE (µs)……....…..6.50
D1 (s)……..…...…2.000
TD0……....…..……1
Channel f1
NUC1……...…..13C
P1 (µs)…….……....10.00

3.4.4. COSY parameters (400 MHz Bruker)

GENERAL
D0 (s)……..…...…0.00000
D1 (s)……..…1.48689
D13 (s)……..…0.0000
D16 (s)……..…..0.00020

In0 (s) ……....……..0.00018720
INF1 (µs) …….187.2000
Channel f1
NUC1……...…..1H
PLUPROG……..…… cosygpgf
TD……...….……...2048
NS…….……...…32
DS……..…….…..8
SWH (Hz)... …….....5341.88
AQ (s)……...…….0.1917428
RG…….……...….64
DW (µs)…….……....…93.600
DE (µs)……....…..6.50

Gradient channel
GPNAM1……..…SINE.100
GPZ %.....10.00
P16 (µs) ……..1000.0
P1 (µs)…….……..10.00
P2 (µs)…….…… 20.00
PL1 (dB)…….…….. -4.00
PL1W (W) ….……..…....47.8998
SFO1 (MHz)….……..…….…100

3.4.5. HMQC parameters (400 MHz Bruker)

GENERAL

D13 (s)…….…0.0004
D16 (s)…….…….0.00020
DELTAL (s)……..…0.0022
In0 (s) ……...……...…..0.0003000
INF1 (µs) ……...60.00
Channel f1
NUC1……...…..1H
P1 (µs)…….....10.50
P2 (µs)…….… ….....21.00
PL1 (dB)…….…….…..... -4.00
PL1W (W) ….……..…....23.59780
SFO1 (MHz)….……..…400.131813
PLUPROG……..…… hmqcgpgf
TD……...…..…….....1024
NS…….……..…..…48
DS……..…….…..16
SWH (Hz)... …….....4045.31
AQ (s)……..……..…0.1266
RG…….……..….26008
DW (µs)…….…….....…123.600
DE (µs)…….....…..6.500
D0 (s)……..…..…0.0000030
D1 (s)……1.50000
D12 (s)……0.0034

3.4.6. HMBC parameters (400 MHz Bruker)

GENERAL

D13 (s)……0.0004

D16 (s)……0.00020

DELTAL (s)……0.0022

In0 (s) ……0.0003000

INF1 (µs) ……...60.00

Channel f1

NUC1……1H

P1 (µs)……10.50

P2 (µs)…… ….....21.00

PL1 (dB)…….... -4.00

PL1W (W) ……23.59780

SFO1 (MHz)……400.131813

PLUPROG…… hmbcgpgf

TD……....4096

NS……64

DS……..16

SWH (Hz)... ……..5208.33

AQ (s)……0.3932

RG……16384

DW (µs)……96.0000

DE (µs)……..6.500

D0 (s)……0.0000030

D1 (s)……1.50000

D12 (s)……0.0034

4. RESULTS and DISCUSSION

4.1.1. Section (A)

The treatment of 8-choloro-3-(1-phenyl-ethylamino)-cyclooct-1-encarbonitrile **1** with (s)-α-methyl-banzylamine **2** would provide chemo-selective substation products **3** and **4**. By Altundaş`s group, **1** and **2** were dissolved in DCM and NEt_3. The reaction mixture was refluxed for 2 days under nitrogen atmosphere (Scheme 4.1). After the usual workup, ^{1}H-NMR from the crude showed no starting material or expected substitution products **3** and **4** but there was a new compound. In the NMR spectrum recorded after the reaction, there was an AA'BB' system which is not related to expected products **3** and **4**. This unexpected compound **X** was also observed in the different substitution reactions (Scheme 4.2) under similar reaction conditions. After the chromatographic separation of the crude materials supplied by Nejat Arçelik, we conducted the structural determination of this unknown compound **X** by using ^{1}H, ^{13}C, DEPT-135, DEPT-90, COSY, HMQC and along with Mass and IR.

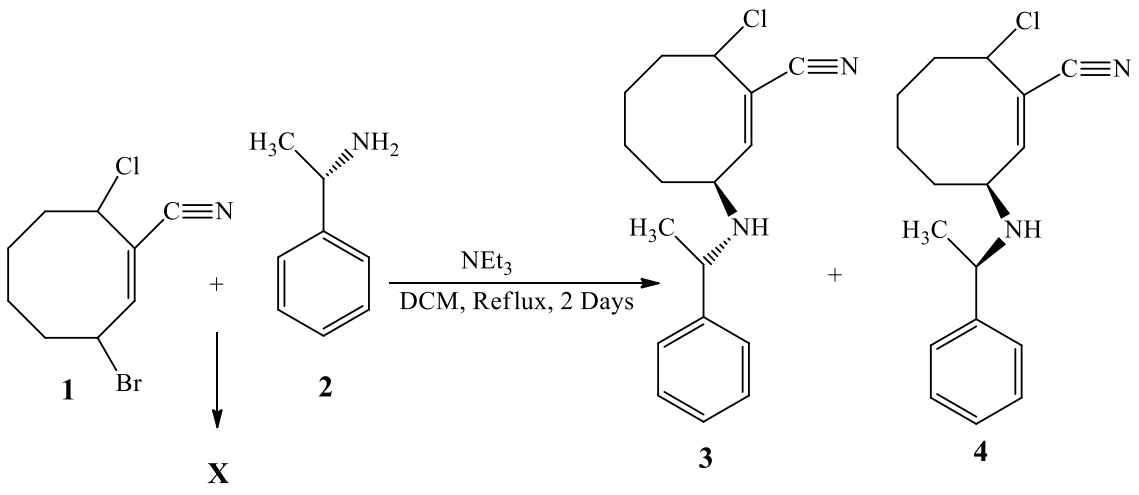

Scheme 4.1. Reaction (**A**), **1** and **2** starting compounds, **3** and **4** expecting compounds.

Synthesized by group the other reactions show in scheme 4.2 with the different materials and different at conditions, we obtained the same molecule.

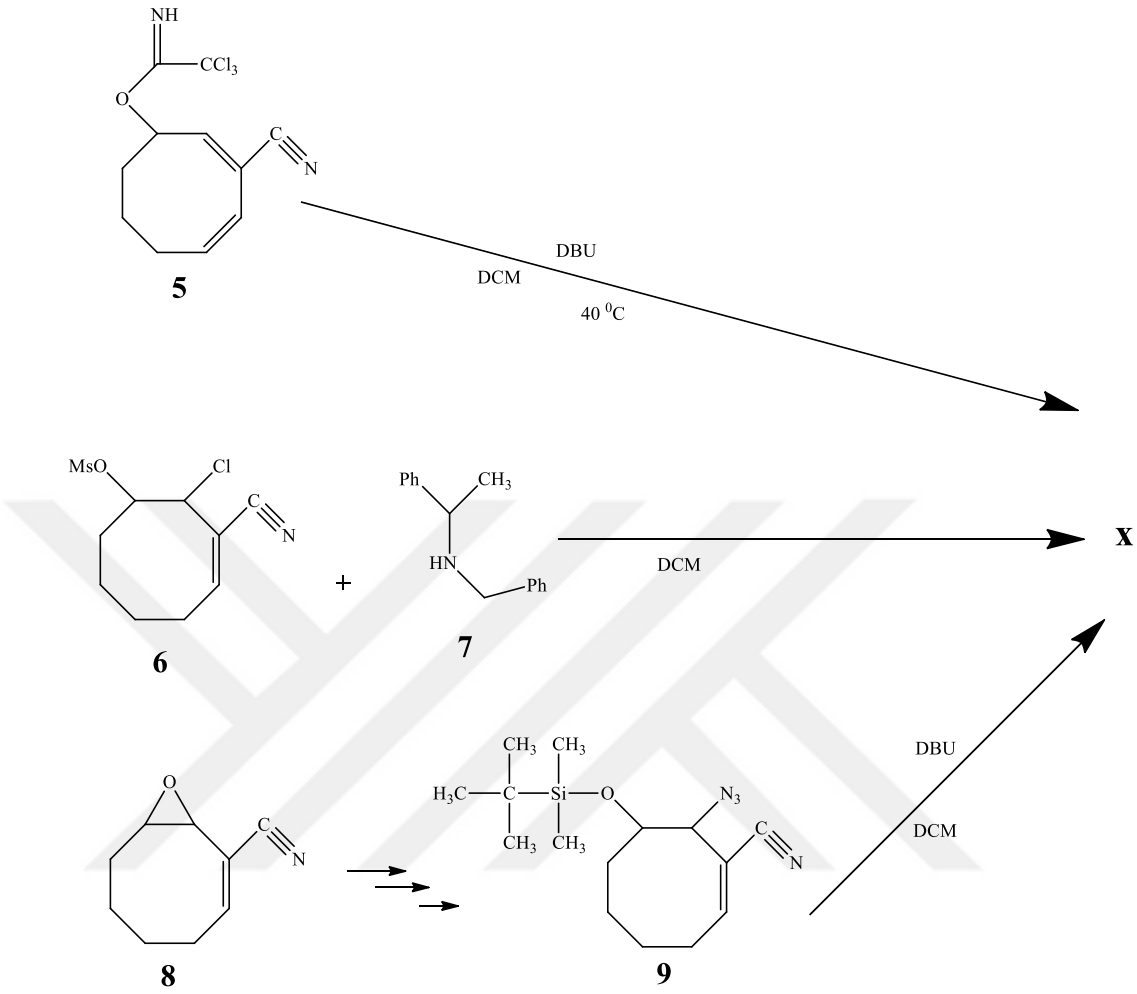

Scheme 4.2. The other reactions which result in **X** molecule

4.1.2. Elucidation of the structure of X molecule (^{1}H-NMR)

^{1}H-NMR spectrum of **X** was given in Figure 4.1. To determine the **X** molecule structure, one and two dimensional spectral data was reported.

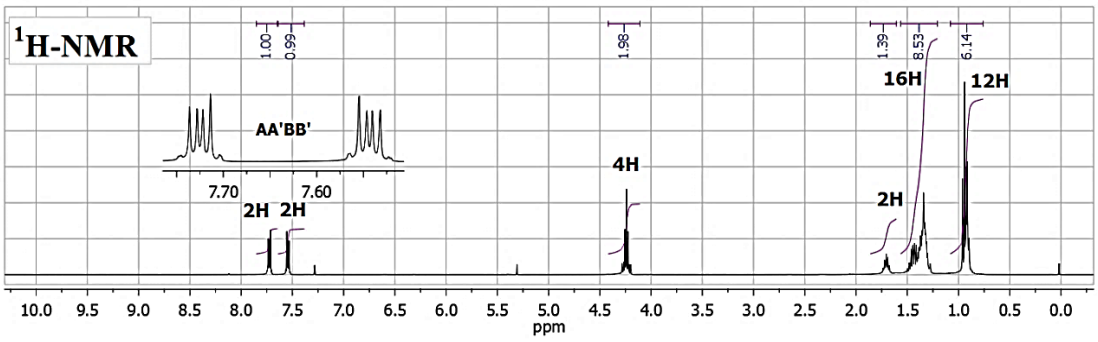

Figure 4.1. ^{1}H-NMR spectrum of **X** molecule with 400 MHz NMR instrument.

The signal group in aromatic region (7.50-7.80 ppm) shows an AA'BB' system, in which corresponds to four protons. So integration ratios indicate totally 38 protons in different regions. The following below statements indicate all protons in the ^{1}H-NMR spectrum of **X** molecule;

* 4 protons in the aromatic region.
* 4 protons connected to any nucleophilic group.
* 30 protons in the aliphatic region.

In the expanded of ^{1}H-NMR spectrum of **X** molecule (Figure 4.2); we can see more accurately recognize the location and type of protons.

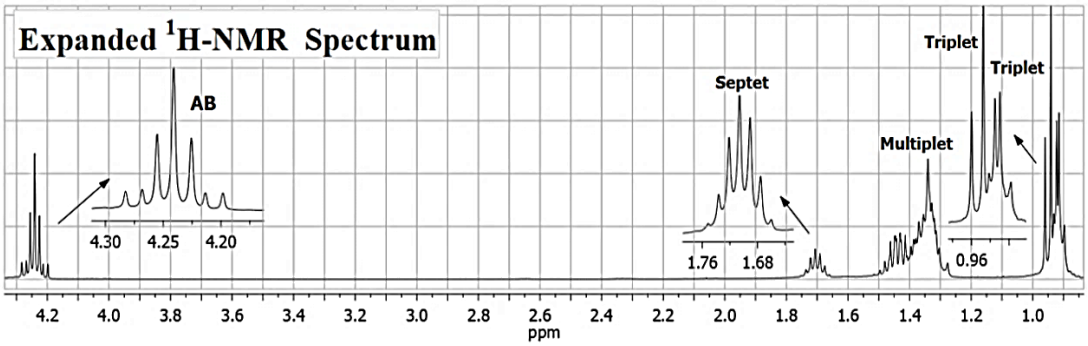

Figure 4.2. Expanded ^{1}H-NMR spectrum of **X** molecule

In the expanded ^{1}H-NMR spectrum, the signal at ~ 4.25 ppm could be correspond to AB system forming which connected to any nucleophilic group.

The HMQC and DEPT spectra confirmed which the signal at ~ 4.25 ppm exactly belong to two methylene groups bonded to any nucleophilic group.

As show in expended spectrum, the signals in aliphatic region give at 1.6 ppm septet, between 1.2 and 1.5 ppm multipet and at 0.96 ppm two triplets. In aliphatic region, the **X** molecule has almost 30 protons, including; methyls, methylenes groups, which is confirmed with HMQC and DEPT spectra lately.

4.1.3. Interpretion of ^{13}C-NMR and DEPT Spectra of X Molecule

^{13}C-NMR, DEPT-90 and DEPT-135 spectra show each kinds of carbons (methyl, methylene, methine and quaternary).

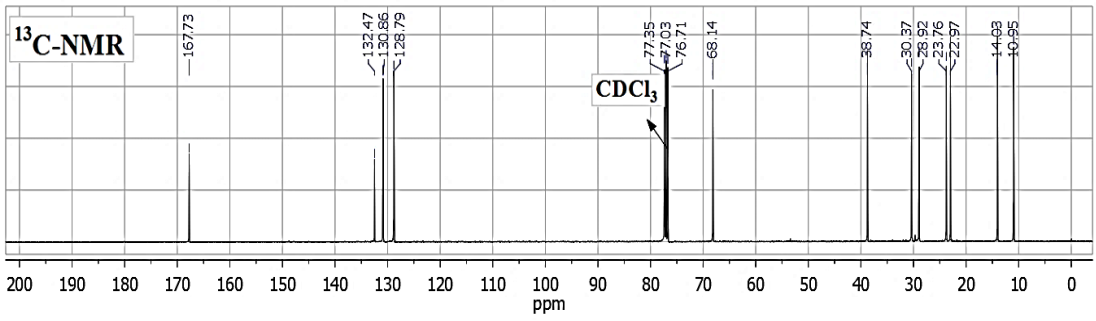

Figure 4.3. ^{13}C-NMR spectrum of **X** molecule with 400 MHz NMR instrument

In ^{13}C-NMR spectrum which is shown in figure 4.3, **X** molecule has twelve carbons signals in different region. According to ^{1}H-NMR and carbons spectral data, we achieved **X** molecule was symmetrical structure. As show in the ^{13}C-NMR spectrum, two signals with weak intensity at 167.73 and 132.47 ppm can be attributed to two quaternary carbons. The signal appearing at 68.14 ppm corresponds to a carbon

connected to any nucleophilic group. Then, the presence of quaternary carbons were confirmed by the DEPT spectra.

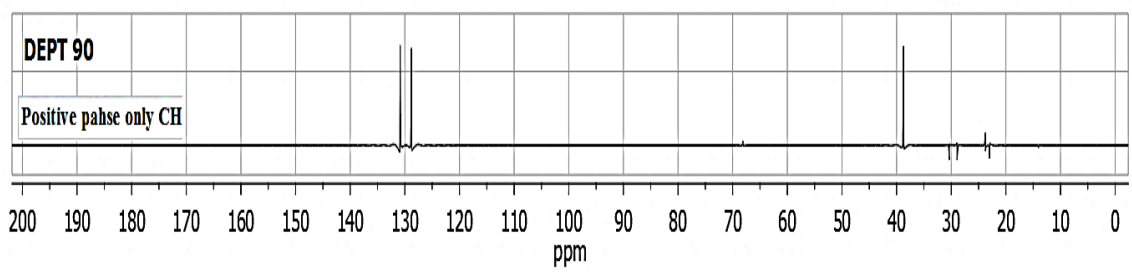

Figure 4.4. DEPT-90 Spectrum of **X** molecule (only CH).

Dept-90 spectrum shows three signals at 128.79, 130.86 and 38.74 ppm corresponded to methine carbons. The signals in Dept-135 spectrum corresponded to methyl (14.03 and 10.95 ppm) and methylene (68.14, 30.37, 28.92, 23.76 and 22.97 ppm) carbons.

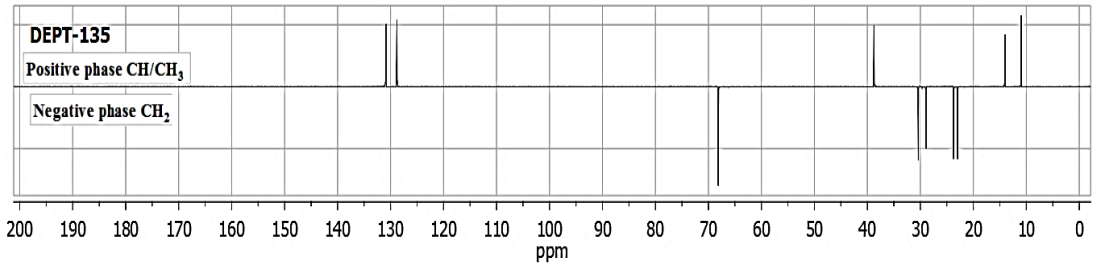

Figure 4.5. DEPT-135 Spectrum of **X** molecule (CH, CH_3 positive and CH_2 negative phase).

4.1.4. Heteronuclear Multiple Quantum Coherence "HMQC"

Heteronuclear multiple quantum correlation spectroscopy is an inverse H-C correlation techniques that allow for the determination of carbon (or other heteroatom) to hydrogen connectivity. HMQC is selective for direct H-C coupling and HMBC will give longer range couplings. Figure 4.6 shows the HMQC spectrum of **X** molecule.

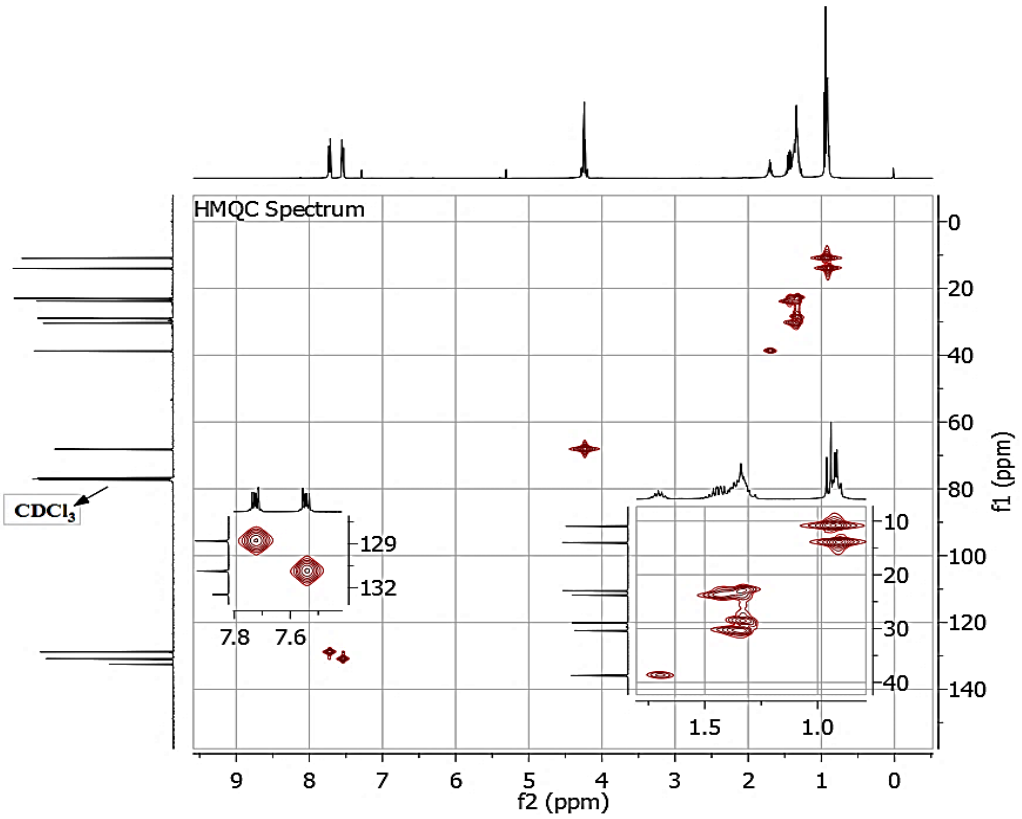

Figure 4.6. HMQC spectrum of **X** molecule

Assignment of all carbons and protons of **X** compound was accomplished through the correlation of the cross peaks in the COSY, HMQC and HMBC spectra. In the HMQC spectrum, at 7.73-7.54 (AA'BB'), 4.24(AB) and 1.71 ppm septet and two triplet at 0.94-0.91 ppm, which correlated with the carbon atoms resonating at 128.79 (*Ar*-CH part of BB'), 130.86 (*Ar*-CH part of AA'), 68.14 (*Nu*-CH_2), 38.74 (aliphatic-CH-), 10.95 (-CH_3) and 14.03 (-CH_3) ppm, respectively.

4.1.5. Correlation Spectroscopy "COSY"

COSY spectra indicate through-bond coupling (^1H-^1H) and can be used to gain structural information about molecules of a wide range of sizes. 2D-NMR uses a sequence of two pulses with a series of different evolution times to determine which nuclear spins are coupled to one another. Figure 4.7 shows the COSY spectrum of **X** molecule.

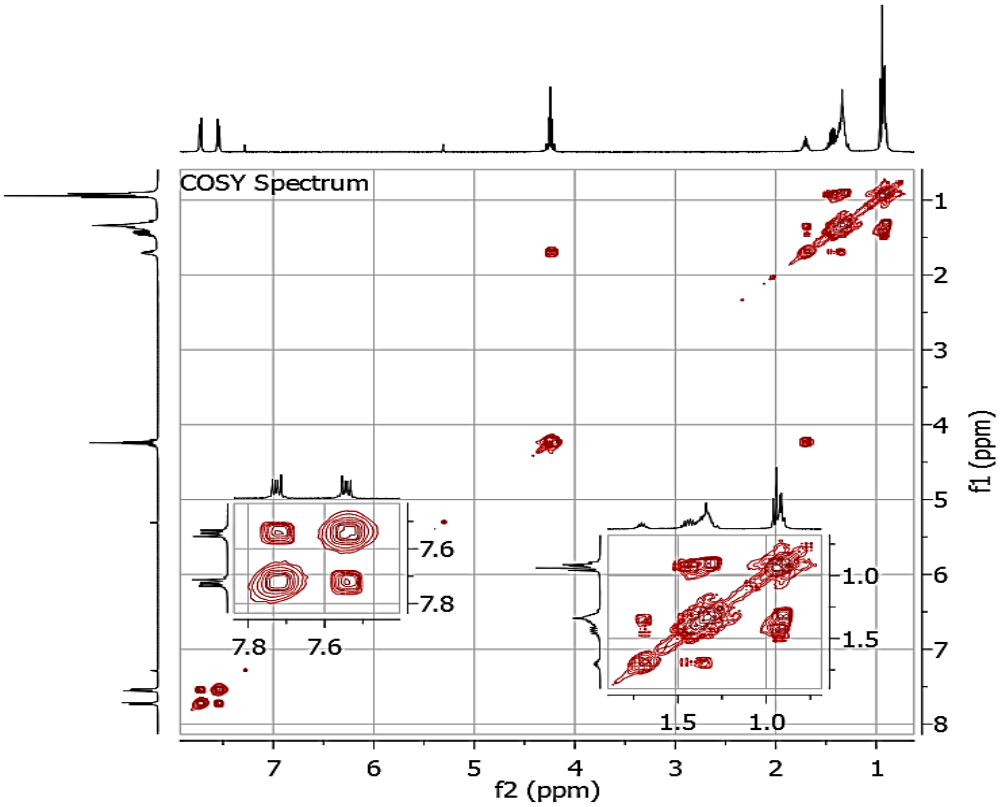

Figure 4.7. COSY Spectrum of **X** molecule

The protons adjacent to each other were determined from the COSY spectrum. In the COSY spectrum, AA' (7.54 ppm) part of the aromatic protons is correlated with BB' (7.73 ppm) part. The methylene protons at 4.24 ppm correlate with the methine proton at 1.71 ppm. On the other hand, the methine proton (1.71 ppm) correlates with the methylene proton at 4.24 and other the methylene protons at ~1.39 ppm. The methyl protons at 0.94 and 0.91 ppm correlate with the methylene protons at ~1.39 ppm.

4.1.6. Heteronuclear Multiple-Bond Correlation Spectroscopy "HMBC"

HMBC is one of the two dimensional experiments. Two-dimensional nuclear magnetic resonance (2D-NMR) provides one of the foremost contemporary tools available for the elucidation of molecular structure, function, and dynamics. HMBC is a long range correlation experiment which provides information about carbons bonded to proton

which are 2, 3 and 4 bonds away. HMBC has applications in every field for identifying and characterizing the structure of compound. Figure 4.8, shows the HMBC spectrum of **X** molecule.

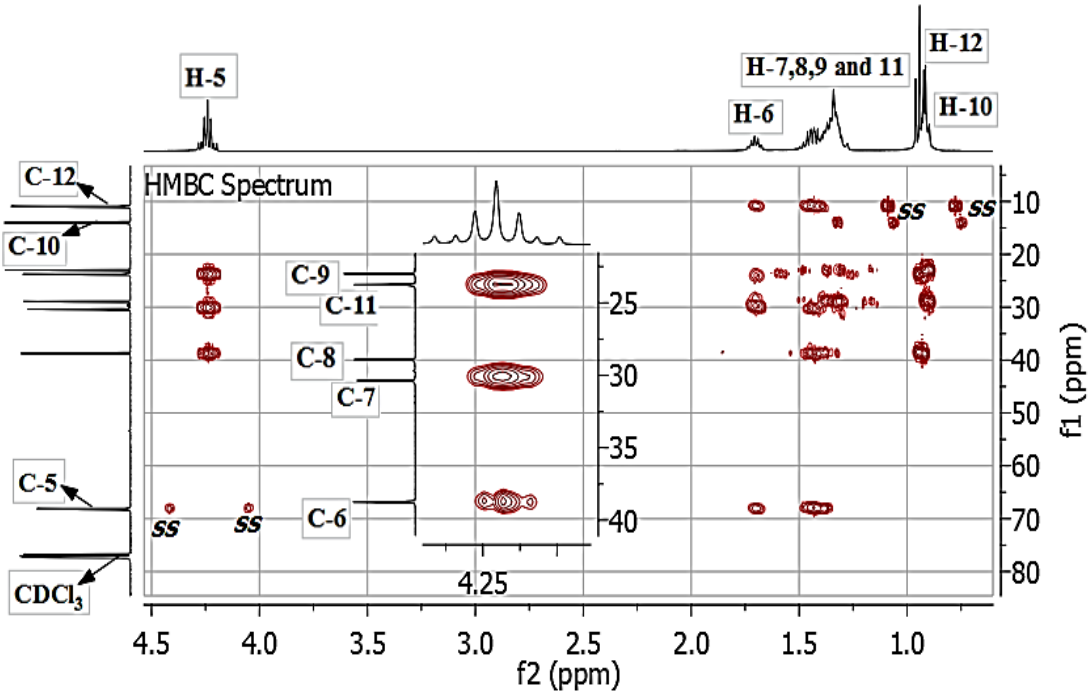

Figure 4.8. HMBC spectrum of **X** molecule

The assignments all proton and carbons of compound **X** were determined by long range (2, 3 and 4 bond) connectivity in the HMBC spectrum. The signals at 167.73 and 132.47 ppm were attributed to the ester and *Ar*-ipso carbons, respectively. The methylene function at 4.24 ppm, which showed correlation with carbon signals at 38.74 (C-6), 30.37 (C-7) and 23.76 (C-11) ppm. The remaining methyl functions at 0.94 and 0.91 ppm in the HMBC spectrum anabled us to assign C-8 and C-9. As a result, the exact structure of the **X** molecule determined by 1D and 2D NMR techniques. In the expanded HMBC spectrum, the exact structure of **X** molecule can be shown in Figure 4.9.

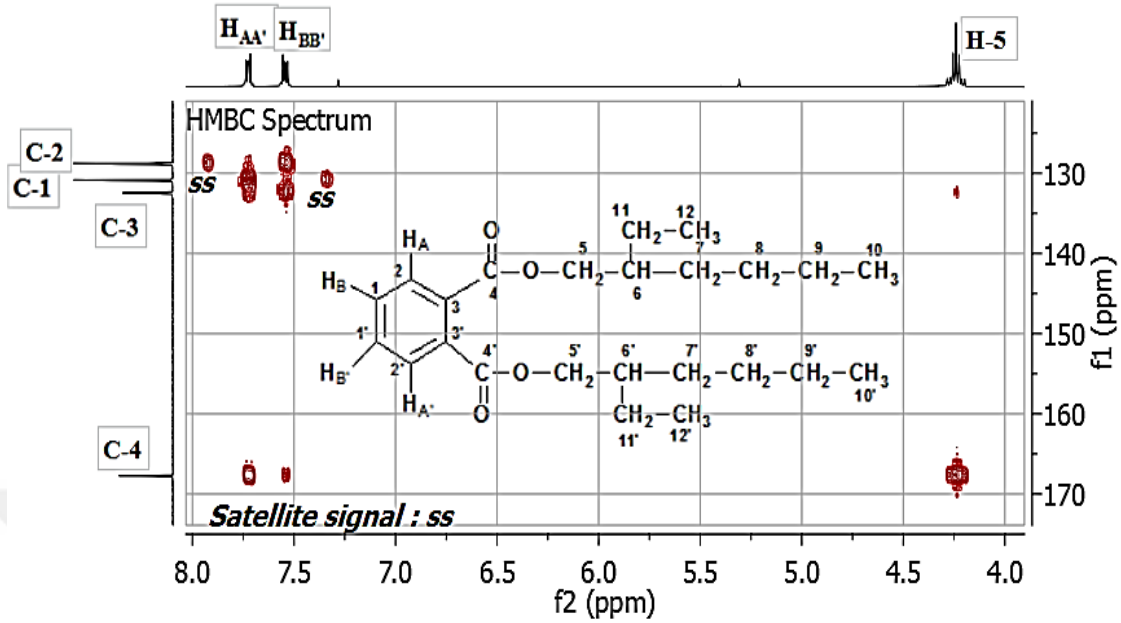

Figure 4.9. The expanded HMBC spectrum of **X** molecule

Compared to the structure of the starting materials, the structure of **X** molecule is quite surprising. Comparing with starting materials and reaction conditions, the oxygen has been observed **X** structure would be shocking. We used more spectroscopic methods for confirmed this structure. We were guessing that the **X** molecule was a symmetrical aromatic compound containing exocyclic double bonds bound to the nitrogen atom as the following Figure 4.10.

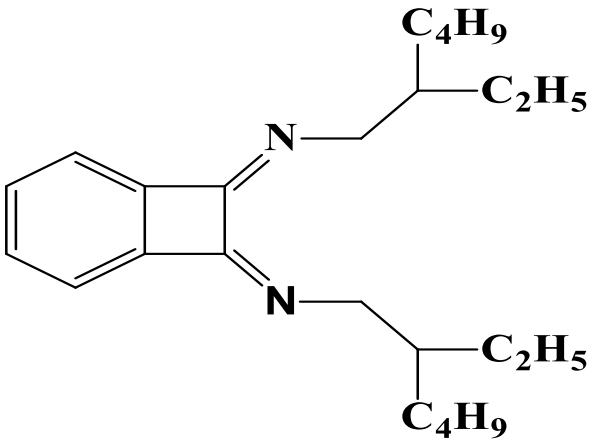

Figure 4.10. Guessing **X** molecule structure

For confirmation of the molecule structure which is shown figure 4.16 we used NMR shift reagent [Eu(fod)$_3$]. It is forms complex with an organic molecule having nucleophilic group. The proton closer to the complex center will be the most affected, and its resonance will move more to down field. If the NMR shift reagent can form a chelate with the ester group, chemical shifts of the methylenic protons attached directly to the oxygen will be shifted down field. But we did not get the desired results from NMR shift reagents. Figure 4.11 shows the proton NMR and containing NMR shift reagents spectra.

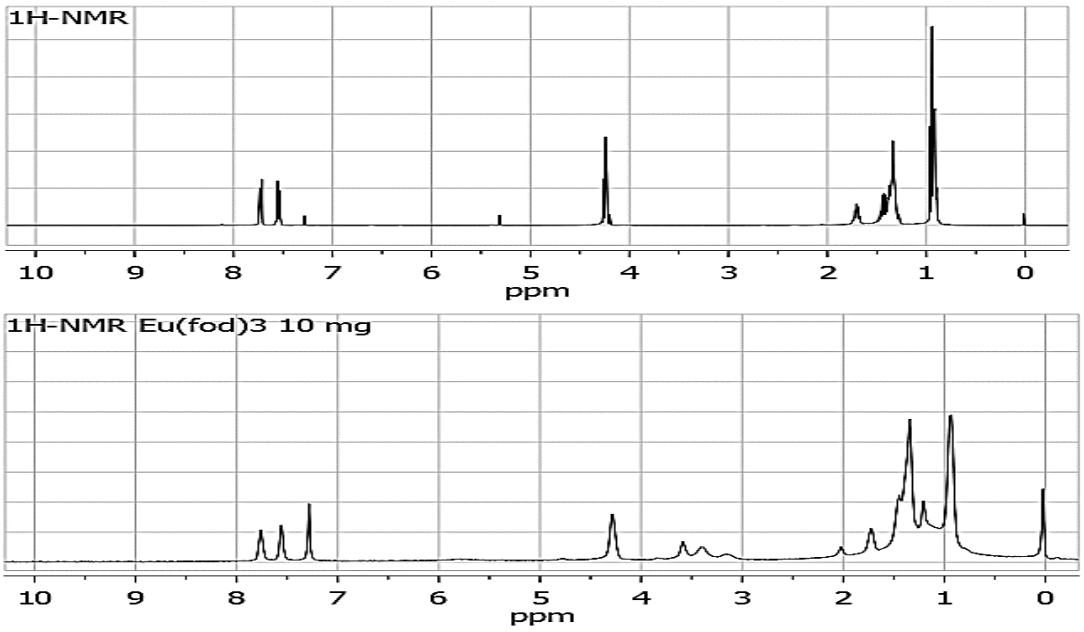

Figure 4.11. ^{1}H-NMR Spectra of X molecule and with Eu(fod)$_3$

However, ^{13}C-NMR spectrum did not agree with the predicted structure of upper molecule. Because, the chemical shift value of methylenic carbon adjacent to the nitrogen could not be at 68.14 ppm.

For **X** molecule, we guessed that is too large molecule and could make complex with [Eu (fod)$_3$] as seen in the Figure 4.12, because it is a large molecule, between **X** molecule and [Eu (fod)$_3$] was not observed a chelate.

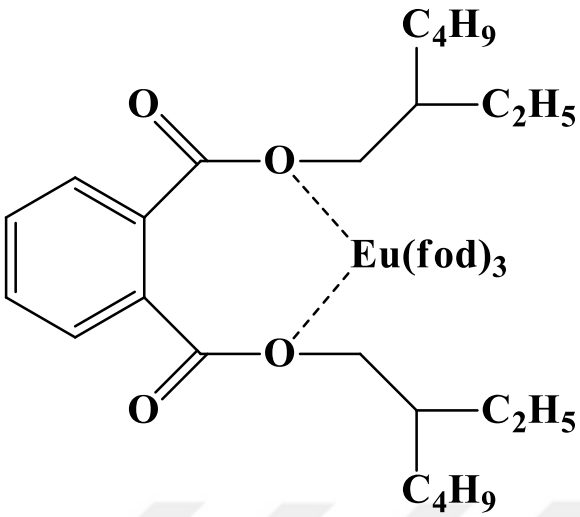

Figure 4.12. Making complex (chelation) with [Eu(fod)$_3$]

4.1.7. Mass Analysis

For mass analysis, we took the **X** molecule weight over once and mass analysis results shown (Figure 4.13) that the molecular weight of **X** molecule is 391.2978 gr/mol.

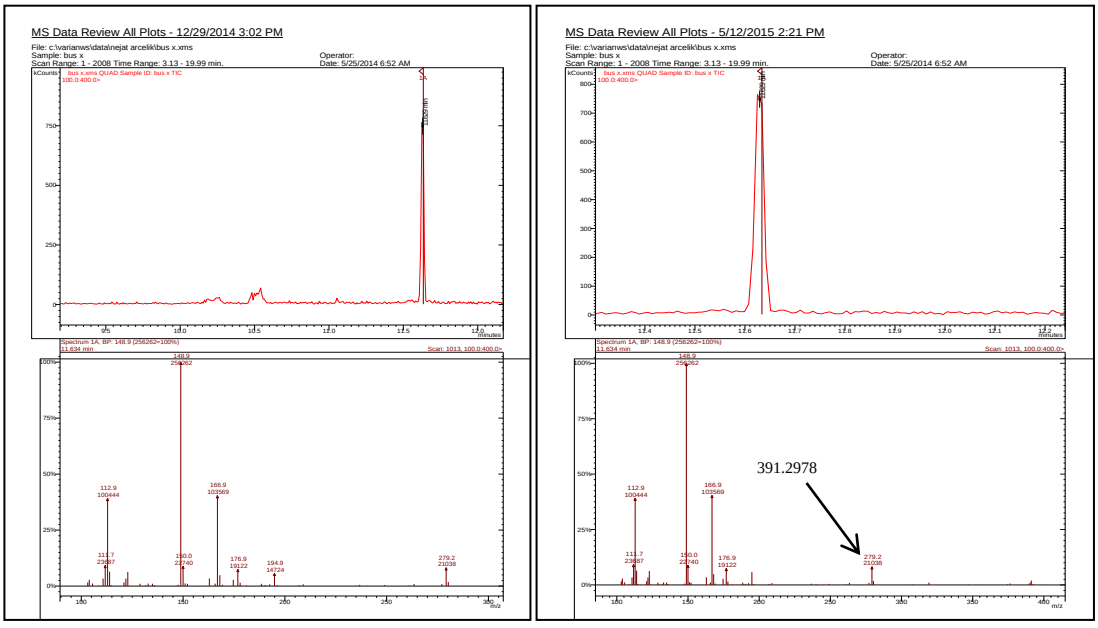

Figure 4.13. Mass analysis spectra of **X** molecule

4.1.8. Infrared Spectroscopy

For more testing and recognized the functional groups of **X** molecule, we took infrared spectrum of it. Figure 4.14 shows the **X** molecule infrared spectrum. IR spectrum confirms the ester group, aromatic and aliphatic groups in our **X** molecule structure.

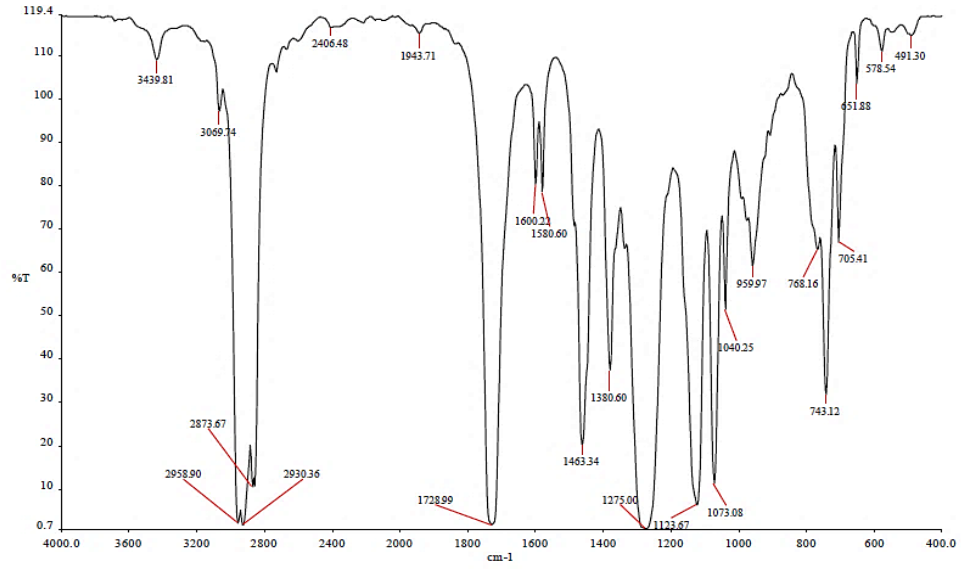

Figure 4.14. Infrared spectrum (IR) of **X** molecule

The Infrared spectrum confirmed the following statements;

* C-H sp^3 stretching's are: 2930.36- 2873.67- 2958.90 cm^{-1}
* C=O has very strong stretching: 1728.99 cm^{-1}
* C-O has very strong stretching: 1275.00 cm^{-1}
*C-H sp^2 aromatic has weak stretching: 1600.22-1580.60 cm^{-1}
* Ortho di-substituted has stretching: 743.12 cm^{-1}

4.1.9. Variable Temperature Unit NMR experiments (VTU)

At dynamic equilibrium, reactants are converted to products and products are converted to reactants at an equal and constant rate. Reactions do not necessarily and most often do not end up with equal concentrations. Equilibrium is the state of equal, opposite rates, not equal concentrations. For this purpose, in order to determine whether dynamic balance **X** molecule, we used VTU control unit. Figure 4.15 shows the ^{1}H-NMR spectra recorded. In the ^{1}H-NMR spectra recorded with 400 MHz Bruker Instrument, high temperatures at 50°C and room temperature are the same. So, we do not discuss about the dynamic equilibrium.

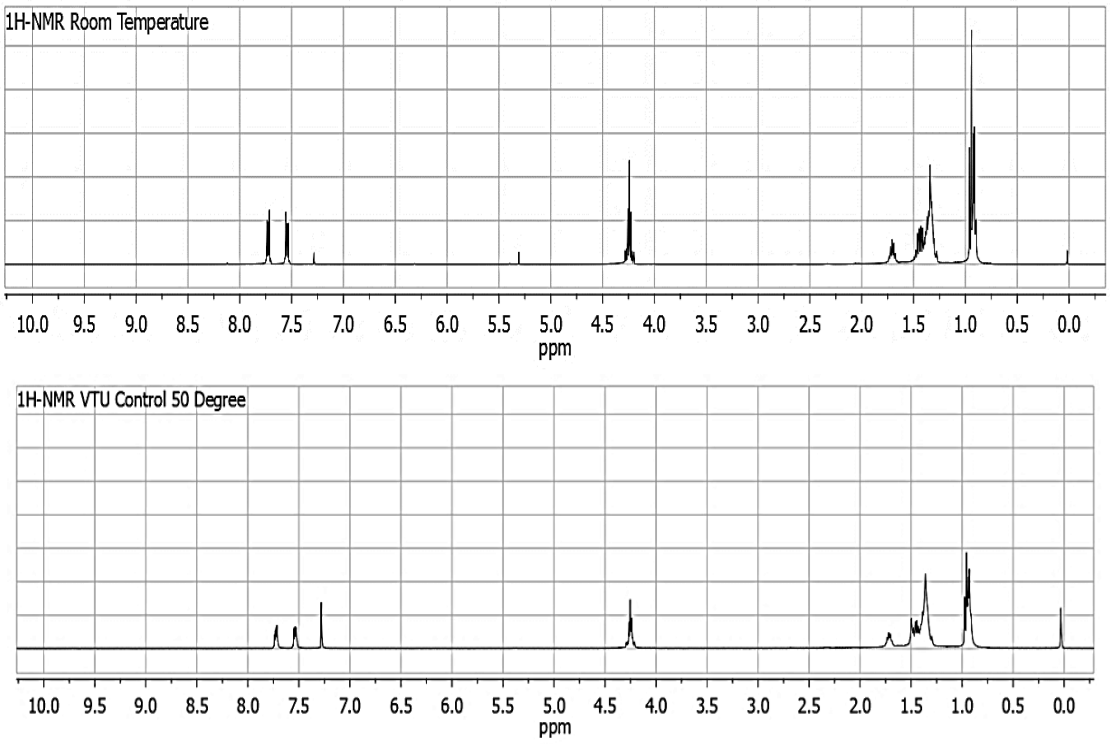

Figure 4.15. The ^{1}H-NMR spectra of **X** molecule recorded at high and room temperature

4.1.10. Solvent Effect

In this part, we thought the molecule **X** according to the starting materials and reaction condition maybe the result of the solvent effect on staring materials. So, we change the solvent in same reaction conditions, In case of, the structure of **X** molecule may result from solvent, the reaction was carried out in Tetrahydrofuran (THF), then took the ^{1}H-NMR. Figure 4.16 shows the the ^{1}H-NMR spectrum of the product obtained had been observed only the starting material.

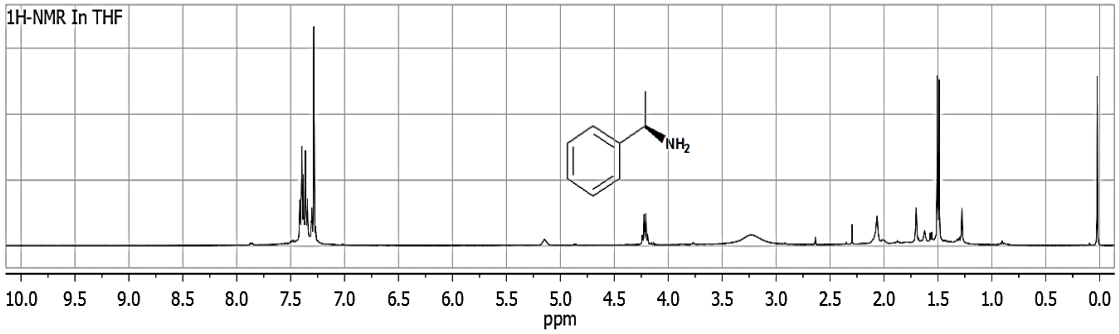

Figure 4.16. ^{1}H-NMR spectrum carried out in THF

In this case the solvent (DCM) maybe considered to be effective in the formation of the **X** molecule. But we couldn't confirm this statement.

The **X** molecule could come from the other sources, the reaction set up in the very common condition, so how could the reaction without the nucleophilic oxygen. So where is the **X** molecule come from?

4.1.11. What is the X molecule?

All spectral data, the structure of the **X** molecule was certainly consistent with the structure of Figure 4.17. The close formula is $C_{24}H_{38}O_4$. It has IUPAC name bis(2-ethylhexyl) phthalate or abbreviated business is **DEHP**. **DEHP** is the most common member of the class of phthalates which are used as plasticizers. It is the dieters of

phthalic acid and the branched-chain 2-ethylhexanol. In general, the chemists use rubber septum in their reaction. Rubber stoppers which seal flasks or bottles. They give an air-tight seal, preventing the ingress of the atmosphere, but are able to be pierced by sharp needles or cannulas. Figure 4.18 shows the common rubber septum. Rubber septa were made from PVC and **DEHP** as plasticizers. These are very flexible to vacuum the reaction in balloons or the glass instruments like them. After using repeatedly of plastics rubber septum and according to reaction conditions like heat or using acids or bases maybe it could be easy to migration the **DEHP** to reaction.

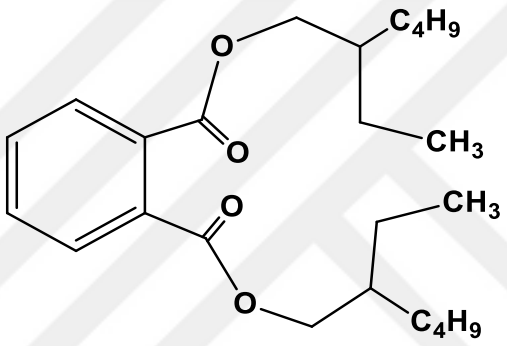

Figure 4.17. DEHP molecular structure

The common rubber septa which are the structural elucidation, we questioned how the DEHP contaminated the reaction. Our partners informed us that they did not see such compound in their laboratory until this work. However we believed that DEHP was extracted into the reaction mixture from the septa which was used to seal the reaction flask.

Figure 4.18. The common rubber septum

In each iteration of the reaction **A**, we couldn't gained the **X** molecule or **DEHP**. So, this statements could be powerful than later which the **DEHP** coming from rubber septum.

4.2.1. Section (B)

We are approached by N. Arçelik to determine the structure of unknown compound was obtained from the epoxide of **10** compound with NaN_3. We are informed that this reaction gave two compounds. After the chromatographic separation of major compound **Y** and minor compound **11** (**Z**) were isolated. Both compounds were liquid. So X-Ray analysis was out of questions.

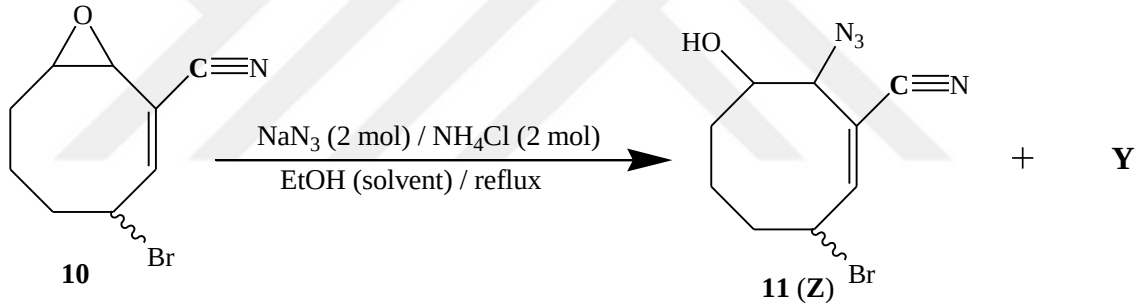

Scheme 4.3. The reaction of epoxide **10** opening with NaN_3

After reaction, two products **11** (**Z**) and **Y** were obtained. The structure of Compound **11** (**Z**) was identified in one and two dimensional NMR techniques. But, the exact structure of the **Y** compound could not be determined.

4.2.2. Elucidation of the structure of Y molecule (^{1}H-NMR)

The ^{1}H-NMR spectrum of staring compound (1), shows the olefinic at 6.8 triplet, the proton next to bromine atom at ~ 4.6 triplet, epoxide protons AB system between 3 and 4 ppm and aliphatic protons multiplet between 1 and 3 ppm in Figure 4.19.

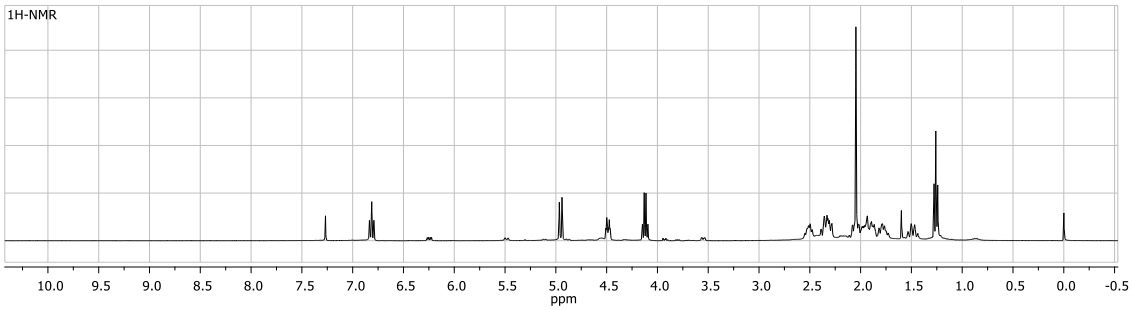

Figure 4.19. ^{1}H-NMR spectrum (impurities-EtOAc) of starting compound **10**

In the ^{1}H-NMR spectrum of **Y** molecule in figure 4.20, the proton signal which is attached to double bond gives doublet of doublets at ~ 6.58 ppm. On the other hand, we observed at 4.80 ppm triplet, 3.61 ppm broad singlet, between 1.5 and 2.5 ppm aliphatic protons. The integration ratios indicate totally 9 protons in different region.

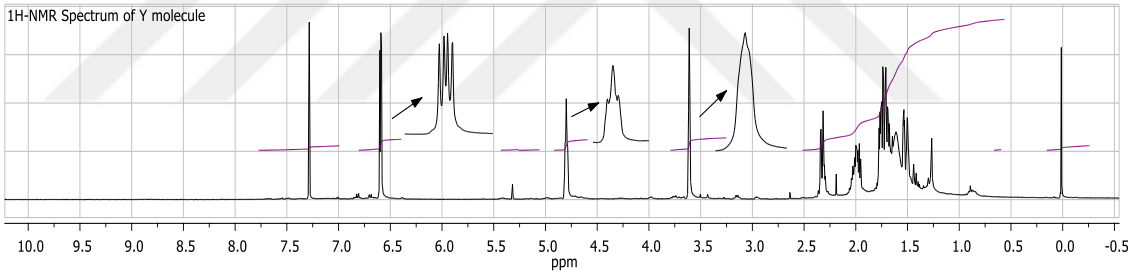

Figure 4.20. ^{1}H-NMR spectrum of molecule **Y**

Each of kind carbon was confirmed by ^{13}C-NMR and DEPT spectra.

4.2.3. Interpretation of ^{13}C-NMR and DEPT spectra of Y molecule

For **Y** molecule, ^{13}C-NMR, DEPT-90 and DEPT-135 spectra show each kinds of carbons (methyl, methylene, methine and quaternary).

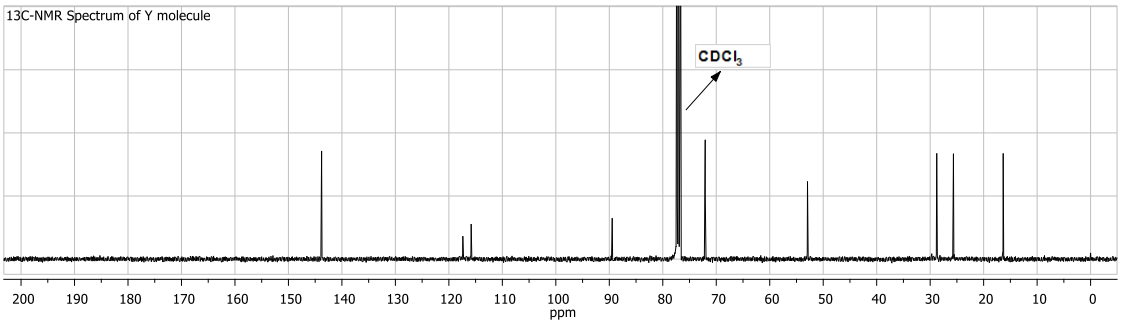

Figure 4.21. ^{13}C-NMR spectrum of **Y** molecule

Totally in ^{13}C-NMR spectrum of **Y** molecule are nine carbons signals in different regions. With considering on the starting materials and the places of the signals in **Y** molecule ^{13}C-NMR spectrum, we found three signals appear at their previous location. The figure 4.22 shows type and the locations of the 3 carbons of **Y** molecule.

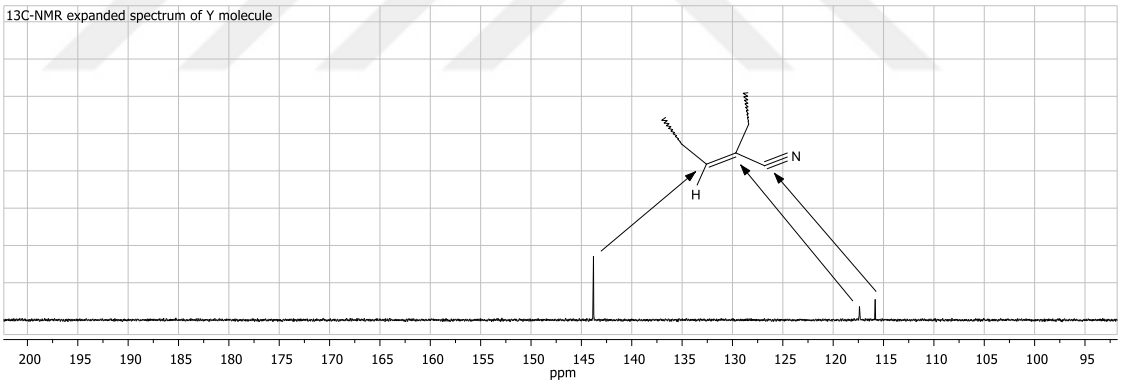

Figure 4.22. ^{13}C-NMR expanded spectrum of **Y** molecule.

The 3 signals appeared in 115.84 ppm, 117.12 ppm and 143.79 ppm, the chemical shifts values closed to the staring compound. As shows in Figure 4.23 we could conclude carbons without changes remain in the **Y** molecule. As continued we took the DEPT-90 and DEPT-135 to determine the type and numbers of the carbons. Figures 4.23 and 4.24 show the DEPT-90 and DEPT-135 respectively.

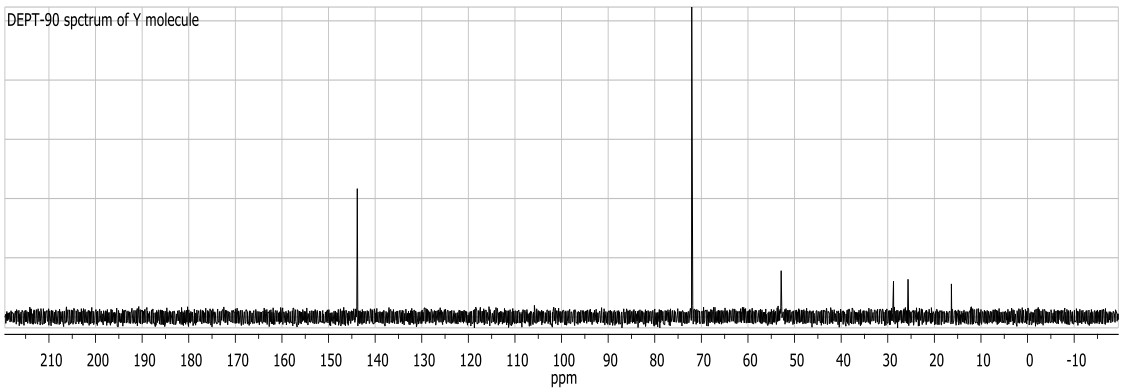

Figure 4.23. DEPT-90 spectrum of **Y** molecule (only CH)

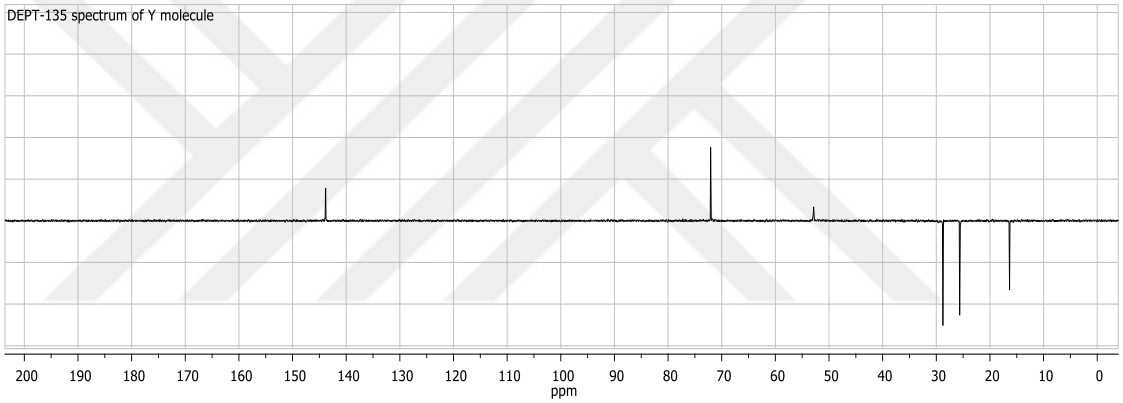

Figure 4.24. DEPT-135 spectrum of **Y** molecule (CH and CH_3 positive and CH_2 negative phase).

After studied the spectra result was; molecule **Y** has no methyl group, 3 methine groups which are appeared in 52.65, 71.78 and 143.79 ppm. The signal of 3 methylene groups appeared in 16.22, 25.37 and 28.52 ppm. The remained 3 quaternary carbon's signal observed at 89.02, 115.84 and 117.12 ppm.

4.2.4. Heteronuclear multiple quantum coherence "HMQC"

In the HMQC spectrum, the signals at 6.58, 4.80 and 3.61 ppm correlated to the carbon's signals at 143.79, 71.78 and 52.65 ppm respectively, and methylenic protons at 2.33, 1.97 and 1.69 ppm correlated to carbon's signals at 28.52, 25.37 and 16.22 ppm. Figure 4.25 shows the HMQC spectrum of **Y** molecule.

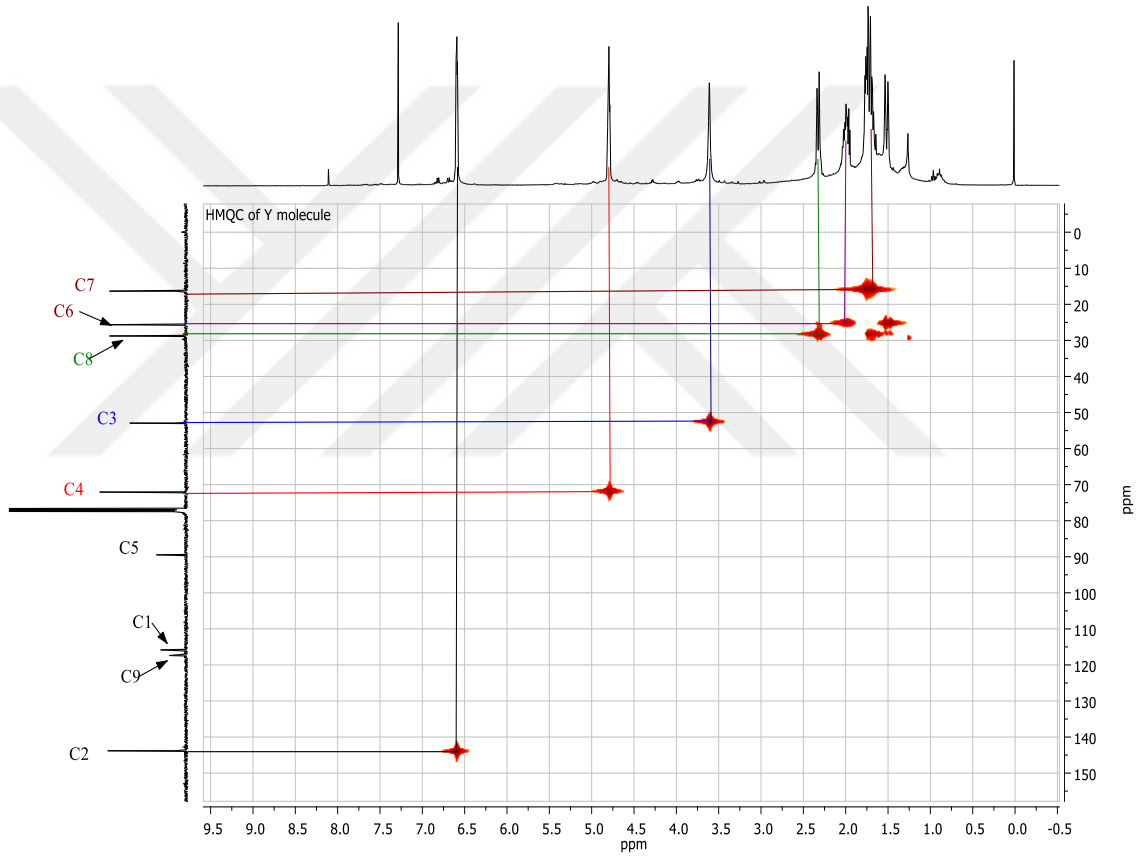

Figure 4.25. HMQC spectrum of **Y** molecule

If we numbered the carbons and the protons 1 to 9, we could have the carbons numbered as the follow the Table 4.1;

Table 4.1. Carbons numbered of **Y** molecule

NO.	^{13}C-NMR Signal (ppm)	^{1}H-NMR Signal(ppm)
C_1	115.84	Quaternary
C_2	143.79	6.58
C_3	52.65	3.61
C_4	71.78	4.80
C_5	89.02	Quaternary
C_6	25.37	1.97
C_7	16.22	1.79
C_8	28.52	2.33
C_9	117.12	Quaternary

4.2.5. Correlation spectroscopy "COSY"

COSY spectra indicate through-bond coupling, and can be used to gain structural information about molecules of a wide range of sizes. 2D-NMR uses a sequence of two pulses with a series of different evolution times to determine which nuclear spins are coupled to one another. Figure 4.26 shows the COSY spectrum of **Y** molecule.

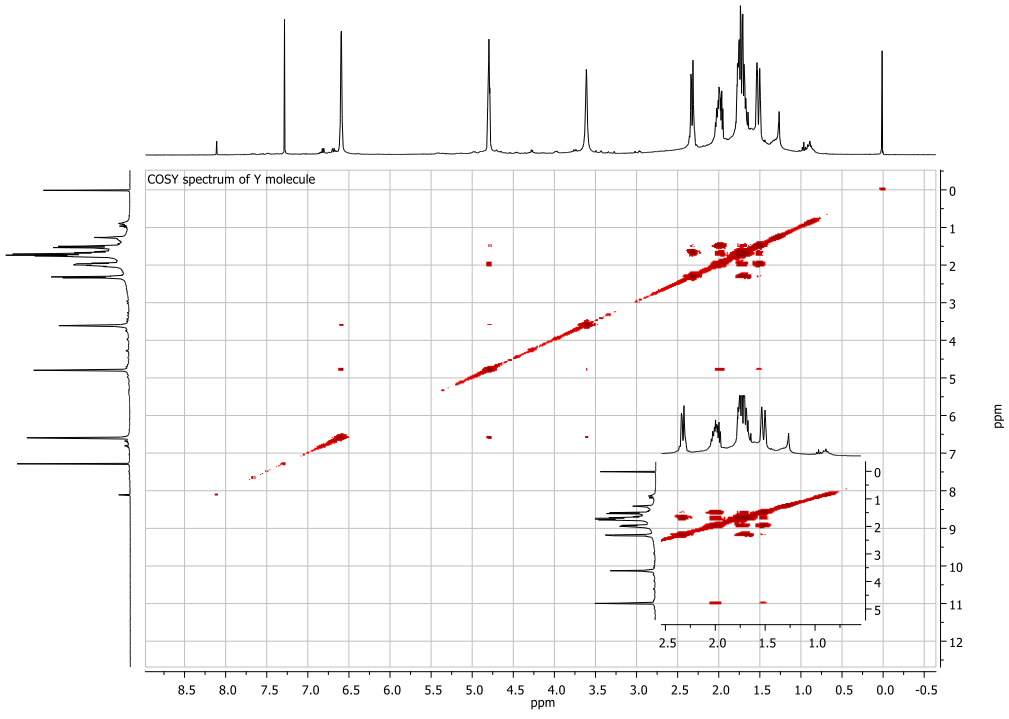

Figure 4.26. COSY spectrum of **Y** molecule

Protons adjacent to each other were determined with the COSY spectrum. In the figure 4.26 shows the adjacent protons in the **Y** molecule. The methylene proton at 1.95 ppm correlated with methylene proton at 1.69 ppm, the methylene proton in 2.33 ppm correlated with the methylene proton at 1.69 ppm, the methine proton in 3.61 ppm correlated with the methine proton at 6.58 ppm which the proton attached to carbons with double bond, the methine proton at 4.80 ppm correlated to the methylene proton at 1.95 ppm and the methine proton at 6.58 ppm correlated with methine protons at 3.61 ppm and 4.80 ppm.

4.2.6. Heteronuclear Multiple-Bond Correlation Spectroscopy "HMBC"

HMBC is one of the two dimensional experiments. Two-dimensional nuclear magnetic resonance (2D-NMR) provides one of the foremost contemporary tools available for the elucidation of molecular structure, function, and dynamics. HMBC is a long range correlation experiment which provides information about carbons bonded to proton which are 2-3 bonds away. HMBC has applications in every field for identifying and characterizing the structure of compound. Figure 4.27 shows the HMBC spectrum molecule.

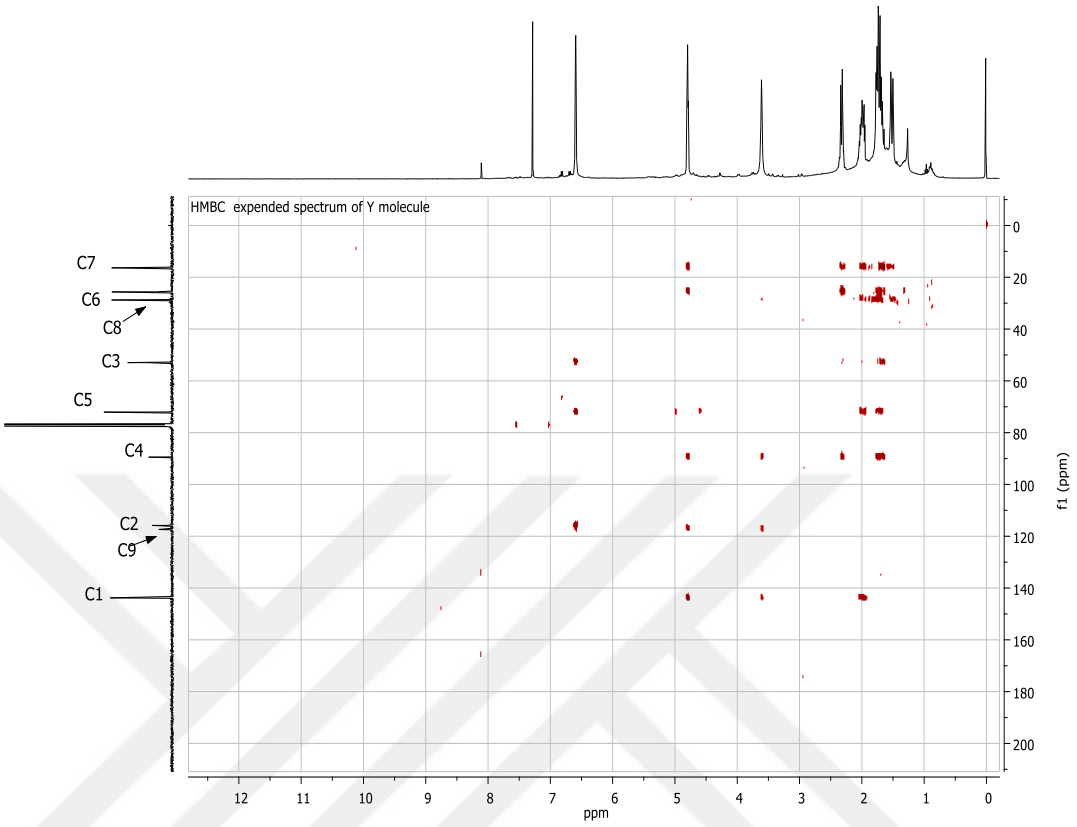

Figure 4.27. HMBC spectrum of **Y** molecule

The proton attached to carbon with double bond correlated with C_3, C_4 and C_2. The proton at 4.80 ppm correlated to C_7, C_6, C_5, C_1 and C_2. The proton at 3.61 ppm correlated with C_2, C_5, C_1 and C_9. The proton at 2.34 ppm correlated with C_7, C_6, C_5 and C_3. The proton at 1.92 ppm correlated with C_7, C_8, C_1 and C_4. The proton at 1.72 ppm correlated C_4, C_8, C_6 and C_5.

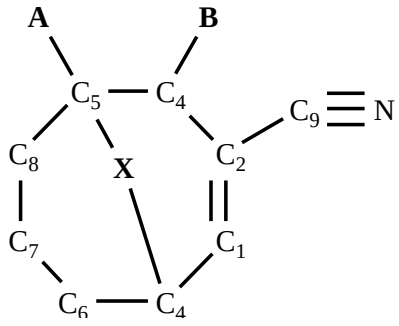

Figure 4.28. The structure of **Y** molecule

According the reaction conditions the groups (X, A and B) have been determined.

4.2.7. Mass Analysis and Infrared spectroscopy

For more testing and recognized the functional groups of **Y** molecule, we took infrared spectrum in Figure 4.29.

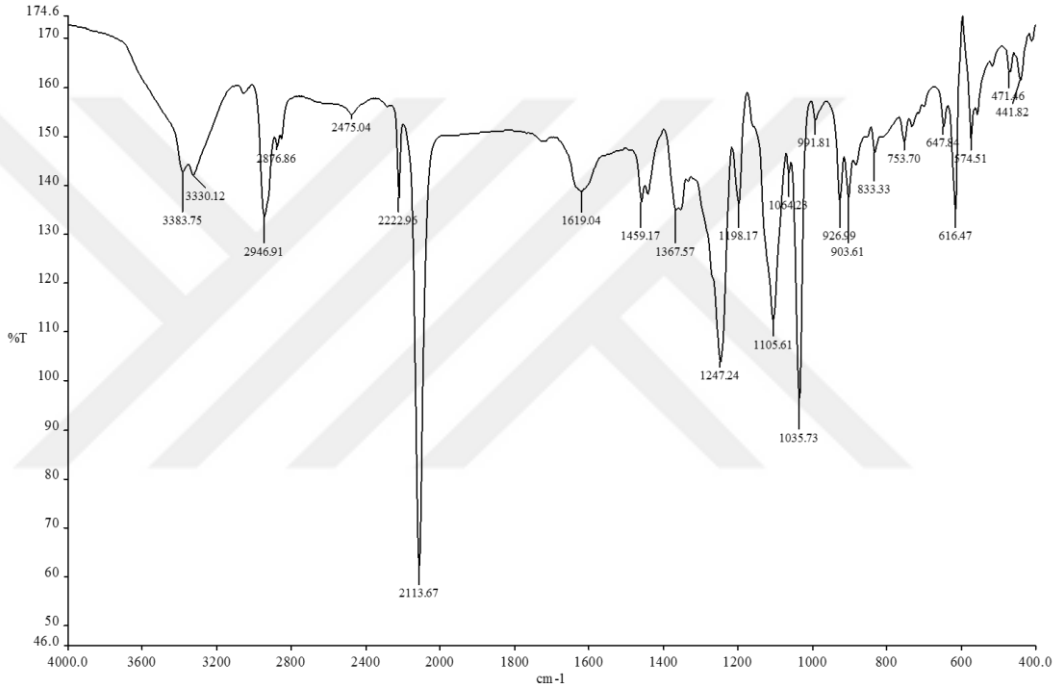

Figure 4.29. Infrared spectrum of **Y** molecule

The Infrared spectra clearly showed the following groups:

* C-H sp^3 stretching's are: 2946.91 cm^{-1}

* N_3 has very strong stretching: 2113.67 cm^{-1} (Eugene Lieber, *et al.* 1962)

* C-O has very strong stretching: 1035.73 cm^{-1}

* N-H has stretching's: 3383.75 cm^{-1}

*O-H has stretching's: 3300.12 cm^{-1}

* C=C has stretching's: 1619.04 cm^{-1}

Mass analysis of **Y** showed 206.97 gr/mol.

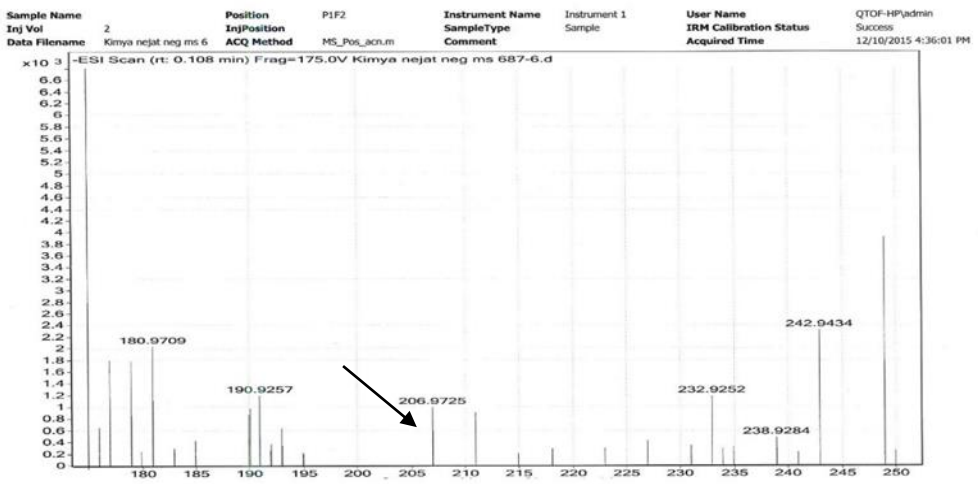

Figure 4.30. Mass analysis of **Y** molecule.

4.2.8. Estimated molecular structures for Y molecule

After all these findings we reached a conclusion that the unknown compound **Y** can be following structures:

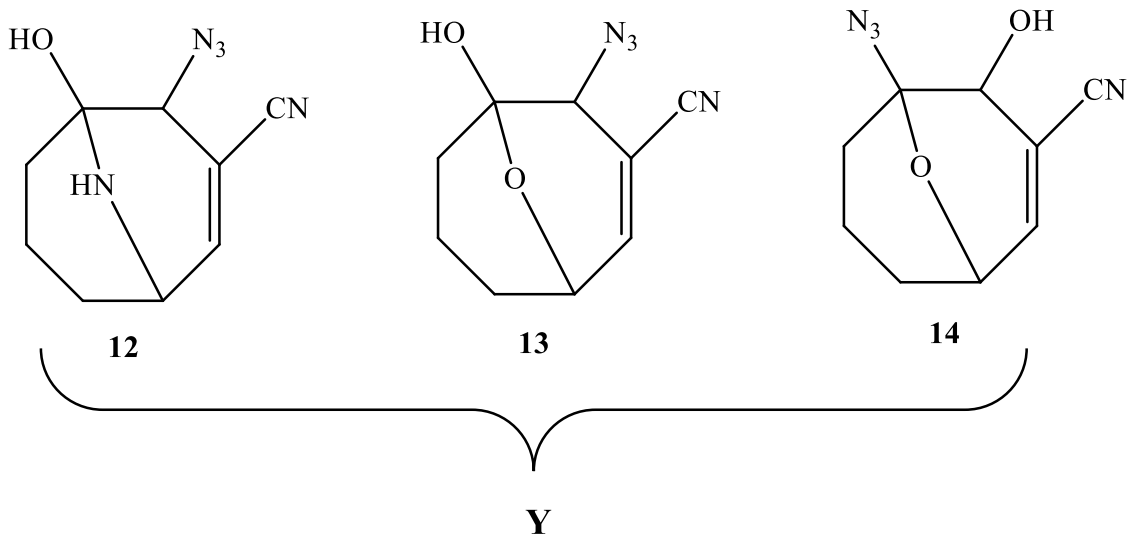

Figure 4.31. Possible structures of **Y** molecule.

According to the spectra and our mass data, we guessed that **Y** can be **12**, **13** or **14**. Because of the quaternary carbon which is bridgehead at 89.02 ppm, if oxygen placed in middle of bridge as shown **13** or **14**, the ^{13}C-NMR signal would be at more than 100 ppm, but in our spectra data this carbon signal is at 89.02 ppm, based on this observation the prediction structure **12** was more acceptable than **13** or **14**.

4.2.9. D_2O exchange.

Acidic protons can be exchanged with deuterium ions. Mixing a compound with D_2O achieves this task. The ^{1}H-NMR spectrum of the exchanged product would be absent of the acidic H peak.

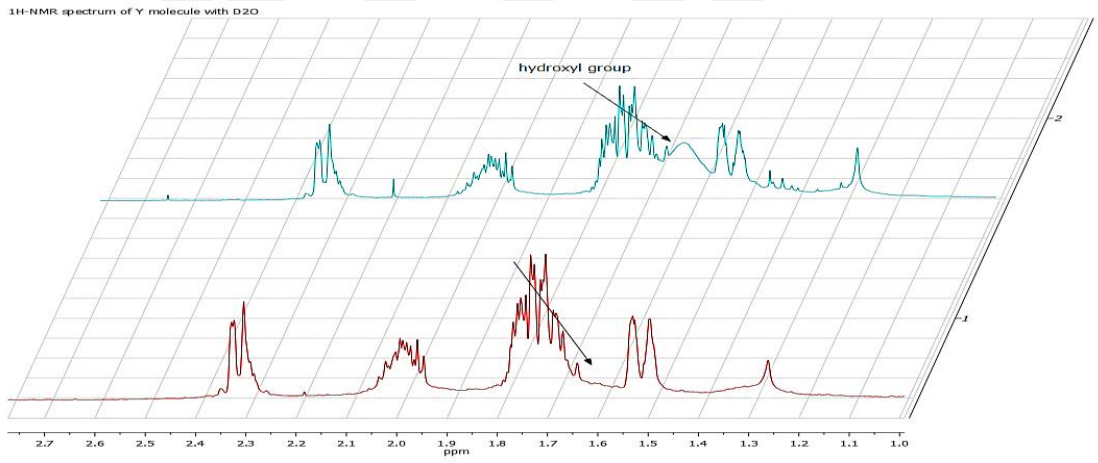

Figure 4.32. ^{1}H-NMR Spectrum of molecule **Y** with D_2O

This ^{1}H-NMR spectrum, the signal at 1.67 ppm corresponded to hydroxyl group. After D_2O exchanging, this signal disappeared, and there were no changes in whole spectrum, that would be mean the hydroxyl group attached to the quaternary carbon at 89.03 ppm.

We thought that the reduction of azide to NH_2 group would solve the problem. For this purposes, the unknown compound was subjected to the reduction reaction with PPh_3 to obtained **15** or **16**, scheme 4.4. However, we informed by our organic chemist partner that the reduction did not give smooth reaction as expected.

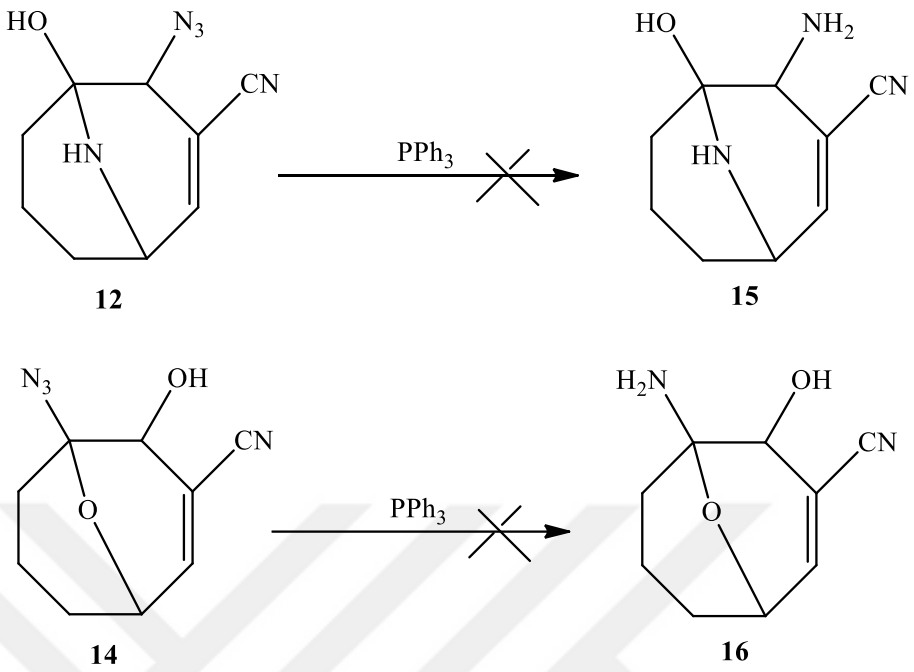

Scheme 4.4. Reduction of azide group

4.3.1. The structural analysis of compound 11 (Z), (minor product)

The minor product which is our expecting one, the structure is determined by NMR techniques as following:

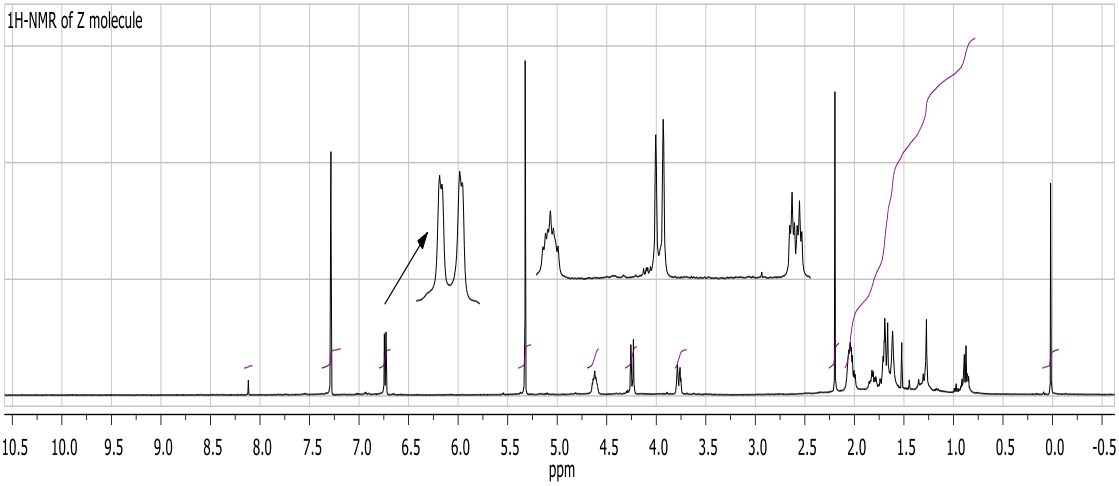

Figure 4.33. ^{1}H-NMR spectrum of Compound **11** (**Z**)

^{1}H-NMR spectrum in figure 4.33.shows the doublet of doublets at ~ 6.74 ppm which its chemical shifts close to starting compound (~ 6.58 ppm). The integration ratios indicate totally 11 protons in different region. The following statements indicate all protons in the ^{1}H-NMR spectrum of molecule **11** (**Z**):

* 1 proton attached to double bond at 6.74 ppm.
* 1 proton at 4.62 ppm.
* 1 proton at 4.24 ppm.
* 1 proton at 3.77 ppm.
* 2 protons at 2.04 ppm.
* 5 protons between 1.4 and 1.8 ppm.

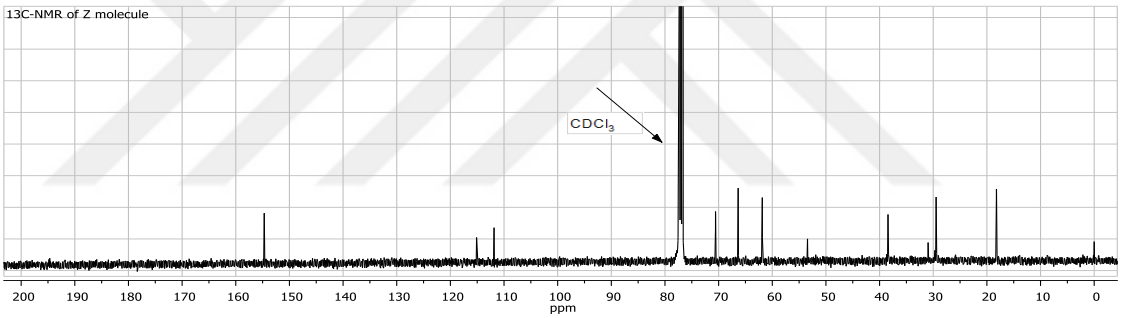

Figure 4.34. ^{13}C-NMR spectrum of molecule **11** (**Z**).

Totally in ^{13}C-NMR spectrum of molecule **11** (**Z**) are nine carbons signals in different regions. With considering on the starting materials and the places of the signals in **11** (**Z**) molecule ^{13}C-NMR spectrum, we found three signals appear at their previous location. The figure 4.34 shown type and the locations of the 3 carbons of molecule **11** (**Z**). The 3 signals appeared in 111.75, 114.91and 154.02 ppm, these are close to staring material chemical shifts. After studied the ^{13}C-NMR spectra the carbons type and the signals placed were determined as the following the Table 4.2.

Table 4.2. Carbon signals and type of molecule **11** (**Z**)

Type	Signals (ppm)
CH	154.02
CH	70.43
CH	65.99
CH	61.92
CH_2	18.08
CH_2	29.16
CH_2	38.24
Quaternary	114.91
Quaternary	111.75

4.3.2. Heteronuclear multiple quantum coherence "HMQC"

The correlations between proton and carbon was determined by HMQC spectrum, is shown in Figure 4.35

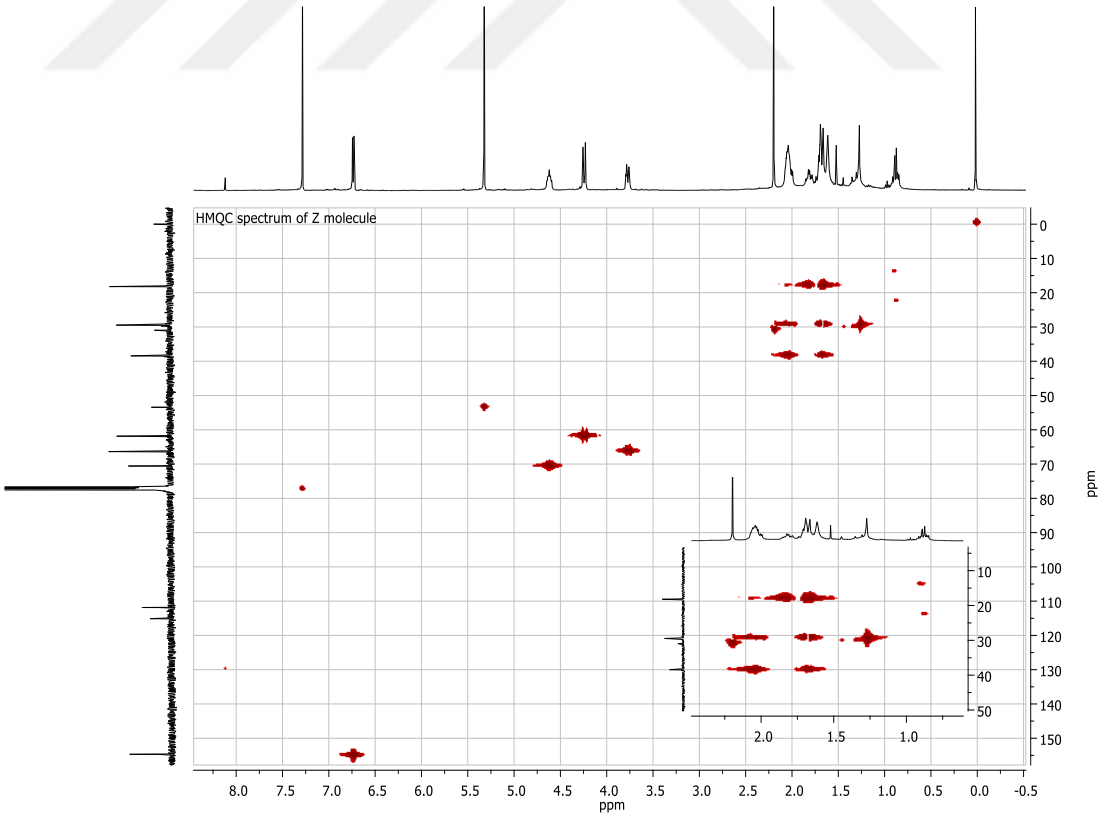

Figure 4.35. HMQC spectrum of molecule **11** (**Z**)

In the HMQC spectrum, at 6.73, 4.62, 4.25 and 3.76 ppm which they are methine carbons correlated to at 154.31, 70.43, 61.92 and 65.99 ppm respectively, and the protons in aliphatic region (1.4-2.04 ppm) correlated to correlate to carbons at 38.40, 29.45 and 18.20 ppm.

4.3.3. Heteronuclear multiple-bond correlation spectroscopy "HMBC"

We reported HMBC spectrum (Figure 4.36) to determine two and three bond the correlation proton and carbon.

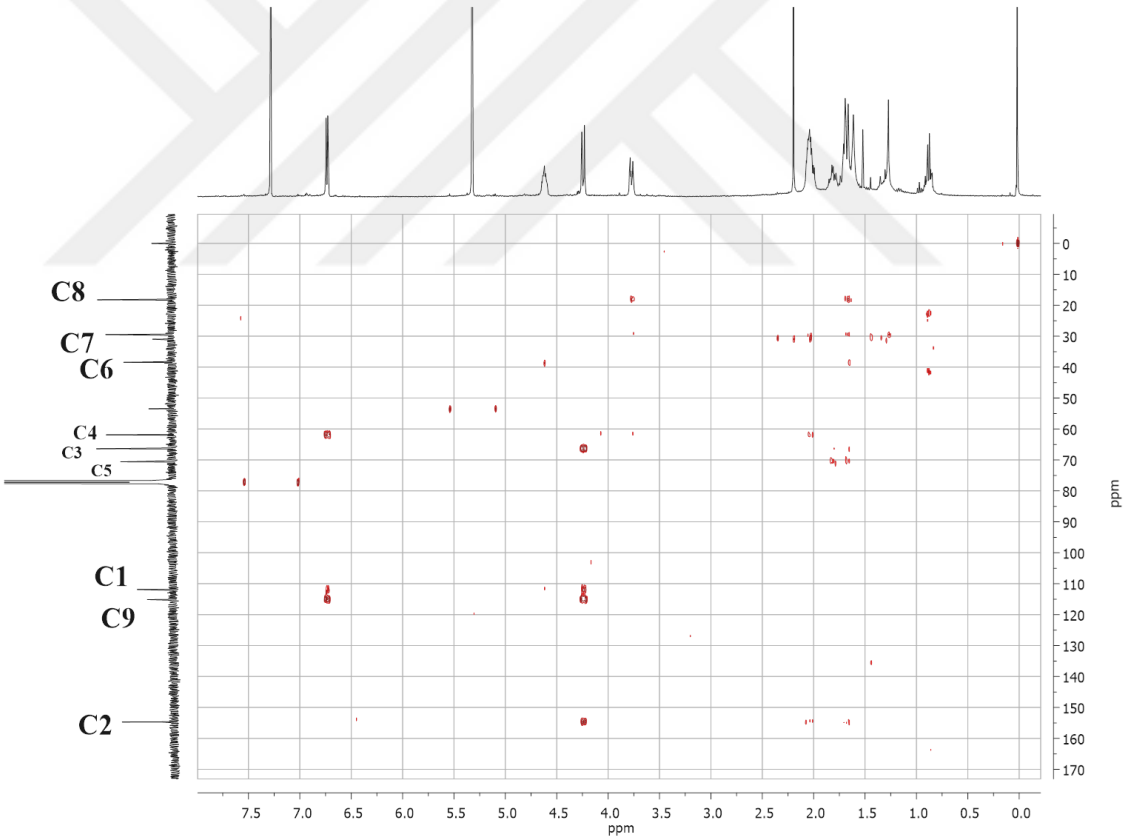

Figure 4.36. HMBC spectrum of molecule **11** (**Z**).

In the HMBC spectrum of molecule **11** (**Z**) were observed, the proton at 6.73 ppm correlated with C_9, C_4 and C_1. The proton at 4.62 ppm correlated to C_6. The proton at 4.25 ppm correlated with C_3, C_2, C_1 and C_9. The proton at 3.76 ppm correlated with C_4

and C_8. The proton at 2.04 ppm correlated with C_7, C_4 and C_2. The protons in aliphatic region between 1.4 and 1.8 ppm C_2, C_8, C_5, C_6 and C_7.

4.3.4. Mass analysis

For mass analysis, we took the molecule **11** (**Z**) weight over once and the result as show in Figure 4.37. The molecular weight is 279.0 gr/mol.

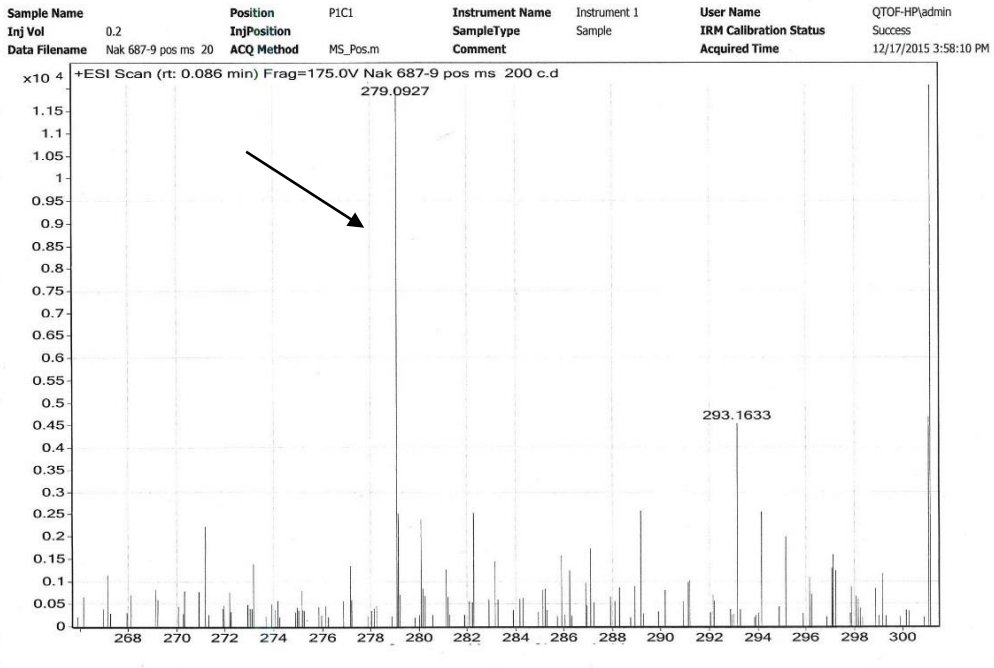

Figure 4.37. Mass analysis of molecule **11** (**Z**)

4.3.5. Infrared Spectroscopy

The IR spectrum of molecule **11** (**Z**) shows the functional group at 2113.67 cm^{-1} as azide group, at 3331.93 cm-1 as hydroxyl group. Although we determined exactly structure of molecule **11** (**Z**), there is still a question in the assessment of the streo-chemical relationship of functional groups.

In the scope of this work, we did not run any experiment for determining of the stereochemistry.

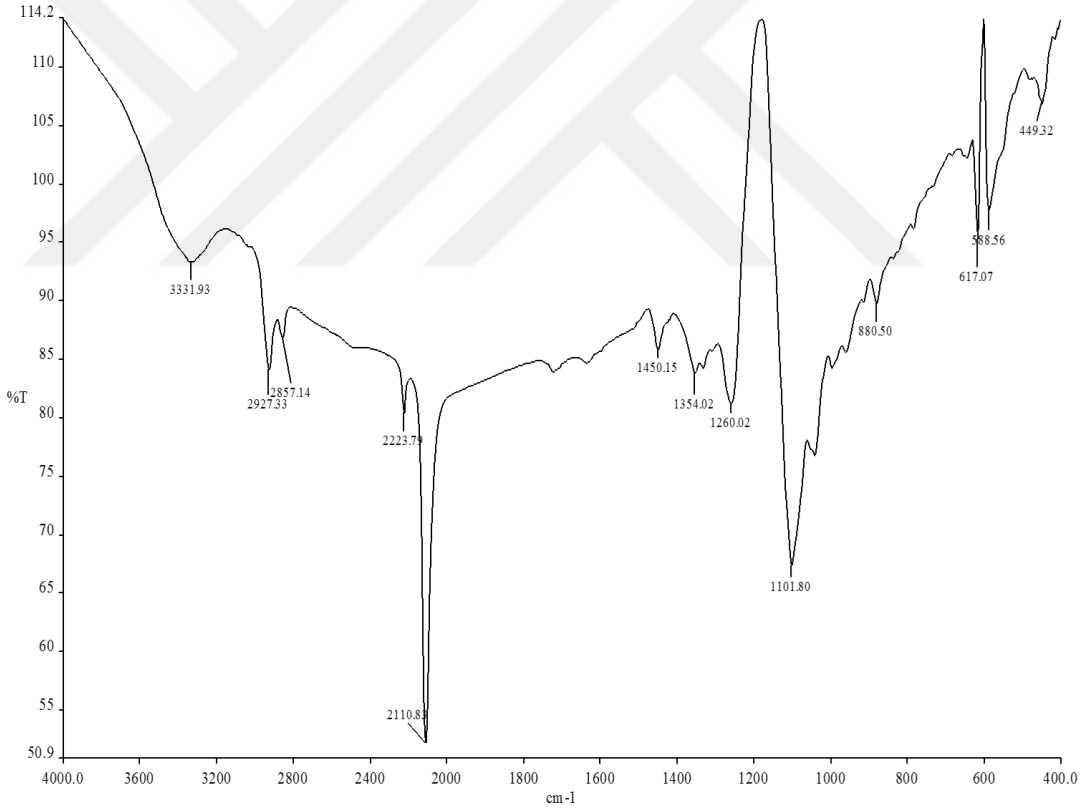

Figure 4.38. Infrared spectrum of molecule **11** (**Z**)

4.3.6. The structure of molecule 11 (**Z**)

To determine the structure of molecule **11** (**Z**), after all the NMR data, mass and IR spectra were taken and the exact structure as following Figure 4.39

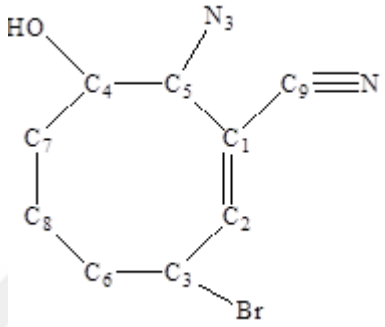

Figure 4.39. The exact structure of molecule **11** (**Z**)

5. CONCLUSION

In this thesis, we used the Advanced NMR techniques structural method to uncover the cyclooctane nitrile derivatives (**X**, **Y** and **Z**).

During the attempt of substitution of chlorine from the cyclooctene **1**, the obtained material was neither desired product nor starting material. It was a new compound to the Altundas`s group. We determined the structure which comes from the plastic rubber and it called **DEHP**, which is used as plasticizer in plastic industries. After finding the structure of this unexpected compound, we concluded that it was extracted from the septa used for sealing the reaction flask. We are also informed by Altundas`s group that they did not observed such compound before. We believe that solvent and base combination in reaction caused **DEHP** extraction into the reaction mixture.

We conducted also the structural elucidation of **Y** which was given by Altundas`s group. During the epoxide opening of **10** with sodium azide provided two different compounds. The major isomer required the advanced NMR studies for the determination of its structure. It was not easy to assess its structure by using only basic ^{1}H-NMR and ^{13}C-NMR techniques. X-ray was not in option in here because the compound was liquid.

We supported our finding with IR and Mass Analysis. Our finding showed that hydroxyl or an azide bonded to quaternary carbon judged by ^{13}C-NMR. The **Y** quaternary carbon should appeared around at 90 ppm. It is still not sure the structure is **12**, **13** or **14**, because the NMR patterns in NMR, the mass spectra will be very helpful to determine the structure, because of the structure **12**, **13** or **14** so closed together corresponded the placing on functional group. Molecule **11** (**Z**) is our expecting product and determined the exact structure of it. The structure of **Y** molecule could predict by using NMR techniques. We did not run any experiment to study the stereochemistry.

REFERENCES

Aboul-Kassim, T. S., 2001. Organic Pollutants in Aqueous-Solid Phase Environments: Types, Analyses and Characterizations: The Handbook of Environmental Chemistry 5E, 1-105.

Abragam, A., 1983. Principles of Nuclear Magnetism: Oxford, UK.

Akitt, J.W., 1992. NMR and Chemistry: An Introduction to Modern NMR Spectroscopy; 3rd ed, Chapman,

ASTM D1239 – 14, 1971. Standard Test Method for Resistance of Plastic Films to Extraction by Chemicals.

Bakhmutov, V. I., 2004. Practical NMR Relaxation for Chemists: John Wiley & Sons, Ltd, Chichester, UK.

Becker, E. D., 1969. High Resolution NMR: Academic Press, Inc.New York,USA.

Bernard. L., 2014. Analytical methods for the determination of DEHP plasticizer alternatives present in medical devices: A review: Talanta 129 - 39–54.

Binsch, G. A., 1969. Unified theory of exchange effects on nuclear magnetic resonance lineshapes. J.Am.Chem.Soc, 91, 1304-1309.

Bloch, F., Hansen, W.W. and Packard, M., 1946. Nuclear induction. Physical Review 69(3-4), 127-127.

Blümich, B., 2005. Essential NMR, for Scientists and Engineers: Springer, New York, USA.

Brian J., 1998. NMR spectroscopy as a tool for structure-based drug design: Progress in Nuclear Magnetic Resonance Spectroscopy 33-109–151.

Cardoza, L.A., 2004. Applications of NMR spectroscopy in environmental science: Progress in Nuclear Magnetic Resonance Spectroscopy 45 -209–238.

Carlson, K., 2010. Toxicity Review of Di (2-ethylhexyl) Phthalate (DEHP). U. S. C. P. S. Commision. Bethesda, MD.

Carrington, A. McLachlan, A., 1967. Introduction to Magnetic Resonance: Harper and Row, New York, USA.

Ceresana., 2008. Market Study: Polyvinyl Chloride." Retrieved Aug. 8, 2011, from http://www.ceresana.com/en/market-studies/plastics/polyvinyl_chloride/polyvinyl-chloride-market-share-capacity-demand-supply-forecast-innovation-application-growth-production-size-industry.html.

Cooper, D.G., 2006. Metabolites from the biodegradation of di-ester plasticizers by Rhodococcus rhodochrous. Science of the Total Environment 366(1): 286-294.

Dixon, W. T., 1972.Theory and Interpretation of Magnetic Resonance Spectra. Springer, New York, USA.

Duer, M. J., 2004. Introduction to Solid State NMR Spectroscopy; Blackwell Publishing Ltd, Oxford, UK.

Ekelund, B., 2010. Evaporative loss kinetics of di-(2-ethylhexyl) phthalate (DEHP) from pristine DEHP and plasticized PVC: Polymer Degradation and Stability 95 - 1789–1793.

EPA, U. S., 1992. Hazard Summary, Bis(2-ethylhexyl) phthalate (DEHP). D. o. A. Radiation.

Ernst, R.R., Bodenhausen, G., Wokaun, A., 1986. Principles of Nuclear Magnetic Resonance in One and Two Dimensions. Oxford, UK.

Eugene Lieber, C. N. R., 1962. Infrared spectra of acid azides, carbamyl azides and other azido derivatives.* Anomalous splittings of the N, stretching bands. Spectrochim Aicetaa, 1 963, T el. 19, pp. 1135t o 114.

Farrar, T. C. and Becker, E. D., 1971. Pulse and Fourier Transform NMR, Academic Press, New York, USA.

Friebolin, H., 2008. Basic One and Two-Dimensional NMR Spectroscopy, 4th ed., Wiley-VCH: Weinheim, New York, USA.

Gemma M. Kirwan., 2008. Generalised 2D-correlation NMR analysis of a wine fermentation: analytica chimica acta 629- 128–135.

Graham, P. R., 1973. Phthalate ester plasticizers-why and how they are used. Environmental health perspectives 3: 3-12.

Grant, D. M., 1996. Harris, R. H. Encyclopedia of Nuclear Magnetic Resonance. John Wiley& Sons Ltd, UK.

Grob, K., 2008. Plasticizers in PVC toys and childcare products: What succeeds the phthalates? Market survey in 2007.Chromatographia 68(3-4), 227-234.

Harris, R.K., 1986. Nuclear Magnetic Resonance Spectroscopy. A Physicochemical View. Longman, London, UK.

Helm, D., 2007. Correlation between production amounts of DEHP and daily intake. The Science of the total environment, 388(1-3): 389-391.

Hennel, J.W and Klinowski, J., 1993.Fundamentals of Nuclear Magnetic Resonance. Longman Scientific, London, UK.

Horn, O., 2004. Plasticizer metabolites in the environment. Water research 38(17): 3693-3698.

Huber, W. W., Grasl-Kraupp, B. and Schulte-Hermann, R., 1996. Hepatocarcinogenic potential of di-(2-ethylhexyl) phthalate in rodents and its implications on human risk. Critical Reviews in Toxicology, **26**(4):365-481.

Jackman, L. M., 1975. Cotton, F. A.; Dynamic Nuclear Magnetic Resonance Spectroscopy, Academic Press, New York, USA.

Katayama, B., 2010. Study on molecular structure and hydration mechanism of Domyouji-ko starch by IE and NIR hetero 2D analysis. J. Mol. Struct, 974 - 179–182.

Keeler, J., 1998, 2002 and 2004. Two-Dimensional NMR.1998, 2002 and 2004, Wiley Publishers,UK.

Keeler, J., Understanding NMR Spectroscopy,John Wiley & Sons, UKA.

Klinowski, J., 2005. New Techniques in Solid-State NMR, Springer, New York, USA.

Kluwe, W. M., 1983. The Carcinogenicity of Di-(2-Ethylhexyl) Phthalate (Dehp) in Perspective.Journal of Toxicology and Environmental Health, 12(1): 159-169.

Koch, H. M., 2006. Di-(2-ethylhexyl)-phthalate (DEHP): human metabolism and internal exposure-an update and latest results. International journal of andrology 29(1): 155-165, discussion 181-155.

Levitt, M.H., 2001. Spin Dynamics: Basics of Nuclear Magnetic Resonance", John Wiley & Sons, UK.

Lin, L. 1998. The use of multivariate analysis to compare peroxisome induction data on phthalate esters in rats. Toxicol. Ind. Health **3**, 25-48.

Madsen, P. L., 1999. Kinetics of di-(2-ethylhexyl) phthalate mineralization in sludge amended soil. Environmental Science & Technology 33(15): 2601-2606.

Malet-Martino,M. and Holzgrabe, U., 2011. NMR techniques in biomedical and pharmaceutical analysis; Pharmaceutical and Biomedical Analysis 55 (2011) 1–15.

Marcilla, A., 2004. Study of the migration of PVC plasticizers; J. Anal. Appl. Pyrolysis 71-457–463.

Monfette, S., 2010. Monitoring ring-closing metathesis: Limitations on the utility of ^{1}H NMR analysis; Inorganica Chimica Acta 363-481–486.

Munowitz, M., 1988. Coherence and NMR. John Wiley & Sons, UK.

Myers, R.J., 1973. Molecular Magnetism and Magnetic Resonance Spectroscopy. Prentice Hall, New Jersey, USA.

Noda, I., 1986. Two-dimensional infrared (2D IR) spectroscopy of synthetic and biopolymers, Bull. Am. Phys. Soc. 31 - 520.

Noda, I., 2006. Kernel analysis for two-dimensional (2D) correlation spectroscopy, J. Mol. Struct. 799-34–40.

Noda, I., 2015. Recent developments in two-dimensional (2D) correlation spectroscopy; Chinese Chemical Letters 26-167–172.

Noda, I., 2000. Progress in 2D correlation spectroscopy in two-Dimensional Correlation Spectroscopy, AIP Press, Melville.

Noda, I., 2006. Progress in two-dimensional (2D) correlation spectroscopy; J. Molecular Structure 799- 2–15.

Noda, I., 2008. Recent advancement in the field of two-dimensional correlation spectroscopy, J. Mol. Struct. 883–884/2–26.

Paudler, W., 1971. Nuclear Magnetic Resonance; Allyn and Bacon, Inc, Boston, USA.

Purcell, E.M. and Torrey, H.C. and Pound, R.V., 1946. Resonance absorption by nuclear magnetic moments in a solid. Physical Review 69(1-2): 37-38.

Roslev, P., 1998. Degradation of phthalate and di-(2-ethylhexyl) phthalate by indigenous and inoculated microorganisms in sludge-amended soil. Applied and Environmental Microbiology 64(12): 4711-4719.

Sandstrom, J., 1982. Dynamic NMR Spectroscopy; Academic Press: London, UK.

Sears, J. K., 1982. Darby the technology of plasticizers. Wiley, New York, USA.

Shaw, D., 1984. Fourier Transform NMR Spectroscopy, 2nd ed. Elsevier Science Publishers B.V, New York, USA.

Shea, K. M., 2003. Pediatric exposure and potential toxicity of phthalate plasticizers. Pediatrics, 111(6): 1467-1474.

Steiner, I., Scharf, L., Fiala, F. and Washüttl, J.,1998. Migration of di-(2-ethylhexyl) phthalate from PVC child articles into saliva and saliva simulant. Food Additives and Contaminants **7**, 812-817.

Stejskal, E. O. and Memory, J. D., 1994. High Resolution NMR in the Solid State, Fundamentals of CP/MAS. Oxford University Press, New York, USA.

Tadeusz, G. 1992. A Convergent One-Pot Synthesis of Secondary Amines via Aza-Wittig Reaction. Synth. Commun. 22(13).

Thomas .E.A., 1962. Infrared spectra of acid azides, carbamyl azides and another azido derivatives. Anomalous splitting of N_3 stretching bands. Spectrochimica Acta, 1063, Vol 19, pp 1135-1144.

Tickner, J. A.., 2001. Health risks posed by use of di-2-ethylhexyl phthalate (DEHP) in PVC medical devices: A critical review. American Journal of Industrial Medicine, 39(1): 100-111.

Tümay Özer, E., 2012. Determination of di(2-ethylhexyl) phthalate migration from toys into artificial sweat by gas chromatography mass spectrometry after activated carbon enrichment, Polymer Testing 31 (2012) 474–480.

Vasavi, Y., 2011. Heteronuclear Multible Bond Correlation Spectroscopy- An Overview. International Journal of PharmTech Research, Vol.3, No.3, pp 1410-1422.

Welle, F. Roland, F., 2004. Study on the migration behavior of DEHP versus an alternative plasticizer.Giggenhauser Straße 35, D-85354.

Wiseman, J.R., 1975. Carbon- 13 Nuclear Magnetic Resonance Spectroscopy in Conformational Analysis of 9-Azabicyclo [3.3.llnonane Derivatives. J. Org. Chem., Vol. 40, No. 22.

Wypych, G., 2004. Handbook of Plasticizers. ChemTec Publishing, Toronto, Canada.

BACKGROUND

I have Bachelor Degree in Pure Chemistry from Urmia University, Oroumieh, Iran in 2002 to 2006. Then several years of practical work experience in the production and analysis of agricultural pesticides and have agricultural pesticides certified formulator types of Iranian Ministry of Agriculture. And have Iran's national standard of quality control certified white cement, then started to study the Master degree in Ataturk University, working on the organic compound specific NMR techniques analysis. My English skill is in advanced level (Toefl grade (84) / GRE (verbal: 148 / quantitative: 170)) and France (Advance): DALF (A2/B1).